European Journal of Medicinal Chemistry

Manuscript Draft

Manuscript Number: EJMECH-D-19-01154

Title: Identification of a new family of pyrazolo[3,4-d]pyrimidine derivatives as multitarget Fyn-Blk-Lyn inhibitors active on B- and T-lymphoma cell lines

Article Type: VSI: Multi-Target Drugs

Keywords: BCR, B-cell receptor; SFK, Src family kinase; ADME, adsorption, distribution, metabolism, elimination; WHO, World Health Organization; CTCL, cutaneous T-cell lymphoma; DLBCL, diffuse large B-cell lymphoma; PTCL, peripheral T-cell lymphoma; HLs, Hodgkin lymphomas; NHLs, non-Hodgkin lymphomas; FDA, Food and Drug Administration; PDB, Protein Data Bank; MD, molecular dynamics; RMSD, root-mean-square deviation; GAFF, Generalized Amber Force Field; THF, tetrahydrofuran; TBAF, tetrabutylammonium fluoride; MTT, 3-(4,5-dimethylthiazol-2-yl)-2,5-diphenyltetrazolium bromide; SAR, structure-activity relationship; HLM, human liver microsomes; PAMPA, parallel artificial membrane permeability assay; GI, gastrointestinal; MR, membrane retention; PME, Particle Mesh Ewald; DMF, dimethylformamide; DMSO, dimethyl sulphoxide; Pd(dppf)Cl2, [1,1'-bis(diphenylphosphino)ferrocene]dichloropalladium (II); DME, 1,2-dimethoxyethane; MM-GBSA, molecular mechanics generalaized Born surface area

Abstract: Abnormal activation of B-cell receptor (BCR) signaling plays a key role in the development of lymphoid malignancies, and could be reverted by the simultaneous inhibition of Lyn, Fyn and Blk, three members of the Src family kinase (SFK).
Fyn and Blk are also promising targets for the treatment of some forms of T-cell non-Hodgkin lymphoma which point to the druggability of SFKs for the treatment of these cancers. We recently identified Si308 as a potent Fyn inhibitor, while preliminary data showed that it might also inhibit Lyn and Blk. Here, molecular modelling studies were coupled with enzymatic assays to further investigate the effect of Si308 on Lyn and Blk. A small library of pyrazolo[3,4-d]pyrimidines structurally related to Si308 was synthesized and tested on human lymphoma cell lines. Compound 2h emerged as a new multitarget inhibitor of Lyn, Fyn and Blk endowed with remarkable antiproliferative effects on human B and T lymphoma cell lines. Its favorable ADME properties make the compound suitable for further developments.

Graphical Abstract (for review)

Click here to download Graphical Abstract (for review): Graphical abstract.docx

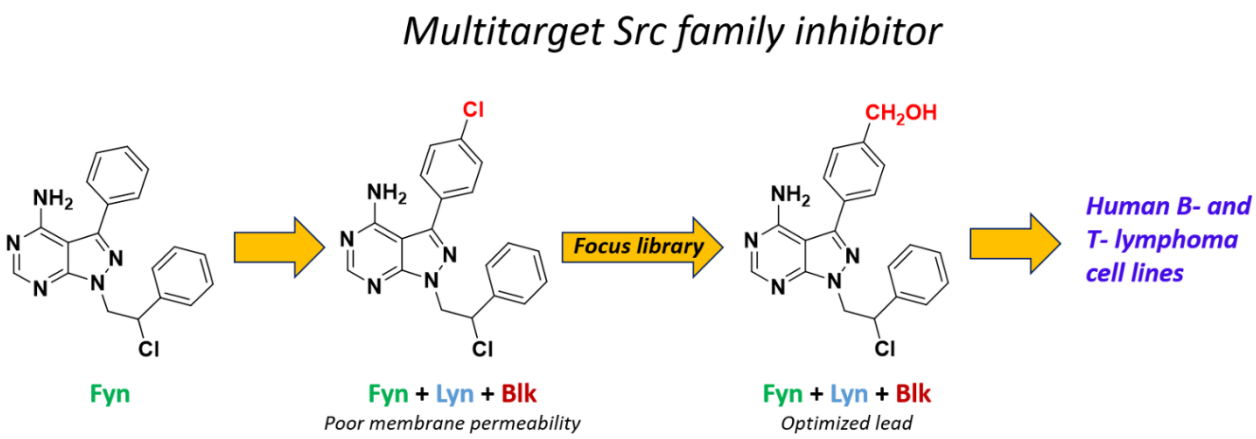

Highlights

- **Si308** inhibits Fyn, Blk, and Lyn, three kinases involved in lymphoma proliferation.
- A focus library of **Si308** derivatives was synthesized and tested on lymphoma cells.
- **2h** is a Fyn, Blk, and Lyn inhibitor with significant antiproliferative effects.
- **2h** has suitable ADME properties, making it a candidate for future developments.

*Manuscript
Click here to download Manuscript: Manuscript.docx Click here to view linked References

Identification of a new family of pyrazolo[3,4-*d*]pyrimidine derivatives as multitarget Fyn-Blk-Lyn inhibitors active on B- and T- lymphoma cell lines

Anna Lucia Fallacara [a], Raffaele Passannanti [a], Mattia Mori [a], Giulia Iovenitti [a], Francesca Musumeci [b], Chiara Greco [b], Emmanuele Crespan [c], Miroslava Kissova [c], Giovanni Maga [c], Chiara Tarantelli [d], Filippo Spriano [d], Eugenio Gaudio [d], Francesco Bertoni [d], Maurizio Botta [a, e, f, *], Silvia Schenone [b]

[a]*Department of Biotechnology, Chemistry and Pharmacy, "Department of Excellence 2018-2022", University of Siena, Via Aldo Moro 2, 53100 Siena, Italy*

[b]*Department of Pharmacy, University of Genoa, Viale Benedetto XV, 3, 16132 Genoa, Italy*

[c]*Istituto di Genetica Molecolare, IGM-CNR, Via Abbiategrasso 207,I-27100 Pavia, Italy*

[d]*Università della Svizzera italiana (USI), Institute of Oncology Research (IOR), via Vela 6, 6500 Bellinzona, Switzerland.*

[e]*Biotechnology College of Science and Technology, Temple University, Biolife Science Building, Suite 333, 1900 N 12th Street, Philadelphia, Pennsylvania 19122, United States*

[f]*Lead Discovery Siena s.r.l., Via Vittorio Alfieri 31, 53019 Castelnuovo, Berardenga, Italy*

ABSTRACT

Abnormal activation of B-cell receptor (BCR) signaling plays a key role in the development of lymphoid malignancies, and could be reverted by the simultaneous inhibition of Lyn, Fyn and Blk, three members of the Src family kinase (SFK).

Fyn and Blk are also promising targets for the treatment of some forms of T-cell non-Hodgkin lymphoma which point to the druggability of SFKs for the treatment of these cancers. We recently identified Si308 as a potent Fyn inhibitor, while preliminary data showed that it might also inhibit Lyn and Blk. Here, molecular modelling studies were coupled with enzymatic assays to further investigate the effect of Si308 on Lyn and Blk. A small library of pyrazolo[3,4-*d*]pyrimidines structurally related to Si308 was synthesized and tested on human lymphoma cell lines. Compound **2h** emerged as a new multitarget inhibitor of Lyn, Fyn and Blk endowed with remarkable antiproliferative effects on human B and T lymphoma cell lines. Its favorable ADME properties make the compound suitable for further developments.

Keywords: Lymphoma, kinase inhibitor**,** pyrazolo[3,4-*d*]pyrimidine, Fyn, Lyn, Blk

Abbreviations[1]

[1] BCR, B-cell receptor; SFK, Src family kinase; ADME, adsorption, distribution, metabolism, elimination; WHO, World Health Organization; CTCL, cutaneous T-cell lymphoma; DLBCL, diffuse large B-cell lymphoma; PTCL, peripheral T-cell lymphoma; HLs, Hodgkin lymphomas; NHLs, non-Hodgkin lymphomas; FDA, Food and Drug Administration; PDB, Protein Data Bank; MD, molecular dynamics; RMSD, root-mean-square deviation; GAFF, Generalized Amber Force Field; THF, tetrahydrofuran; TBAF, tetrabutylammonium fluoride; MTT, 3-(4,5-dimethylthiazol-2-yl)-2,5-diphenyltetrazolium bromide; SAR, structure-activity relationship; HLM, human liver microsomes; PAMPA, parallel artificial membrane permeability assay; GI, gastrointestinal; MR, membrane retention; PME, Particle Mesh Ewald; DMF, dimethylformamide; DMSO, dimethyl sulphoxide; $Pd(dppf)Cl_2$, [1,1′-bis(diphenylphosphino)ferrocene]dichloropalladium (II); DME, 1,2-dimethoxyethane; MM-GBSA, molecular mechanics generalaized Born surface area;

*Corresponding authors.
E-mail addresses: botta.maurizio@gmail.com (M. Botta)

1 INTRODUCTION

Lymphomas are neoplasms that affect the cells of the lymphoreticular or immune system [1]. The World Health Organization (WHO) classifies these diseases with respect to the cells of origin in B-cell, T-cell, and natural killer (NK-) cell lymphomas [2]. Each class includes different subtypes of tumors which are defined on the basis of their peculiarities, such as cellular morphology, molecular lesions and chromosomal alterations [1,3]. The WHO lymphoma classification constitutes the guideline to the correct diagnosis and treatment of these neoplasms, and it is frequently updated by the WHO according to the new genetic and molecular discoveries in the field [1,2]. Lymphomas span from indolent to aggressive on the basis of their growth velocity. Follicular lymphoma and cutaneous T-cell lymphoma (CTCL) are examples of indolent B- and T-cell lymphomas, respectively, while diffuse large B-cell lymphoma (DLBCL) and peripheral T-cell lymphoma (PTCL) are examples of aggressive lymphomas [2].

Lymphomas can be also classified into Hodgkin lymphomas (HLs) and non-Hodgkin lymphomas (NHLs) through a histological analysis. Indeed, HLs are characterized by malignant B-lymphocytes that might evolve into the pathognomonic binuclear Reed-Sternberg cells. In contrast, NHLs are a group of neoplastic diseases characterized by the abnormal proliferation of lymphoid cells, either B- or T-cells, in various sites, including lymph nodes, bone marrow, spleen, liver and the gastrointestinal tract. NHLs are characterized by a great heterogeneity that is usually related to the different stages of differentiation and maturation of these cells [4].

Overall, NHLs account for 90% of all malignant lymphomas, while HLs for the remaining 10%. Evidence showed a dramatic increase in the diagnosis of NHL, which was surpassed only by lung cancer in women and malignant melanoma in both men and women. Thus, much research effort is being spent on understanding the causes of NHLs as well as in finding new therapeutic options [5]. Proven risk factors for NHLs include hereditary immunodeficiency disorders, states of strong immunosuppression (HIV/AIDS, organ transplantation), infectious agents (Epstein-Barr Virus, human T-cell lymphotrophic virus-1, hepatitis C virus, Helicobacter pylori) [6], autoimmune disorders (rheumatoid arthritis, Sjögren's syndrome, systemic lupus erythematosus myositis, Hashimoto's thyroiditis, celiac disease/dermatitis herpetiformis) [3].

The deregulation of the signalling pathways downstream to the B- or T-cell receptors are frequently observed in lymphomas derived from B- or T- cells, respectively [7,8]. Since different members of the Src family kinases (SFKs) play a pivotal role in this signalling, the search for pharmacological agents able to block this class of enzymes is very active. After activation from external factors, BCR triggers multi-enzymatic cascade reactions which promote cell proliferation, growth and survival (Figure 1). In B-cell lymphomas, the two SFKs Lyn and Blk have been recently shown to be essential for the survival of cell lines derived from DLBCL of the germinal center B-cell (GCB) type but not of the activated B cell-like (ABC) [9]. Simultaneous inhibition of the three SFK

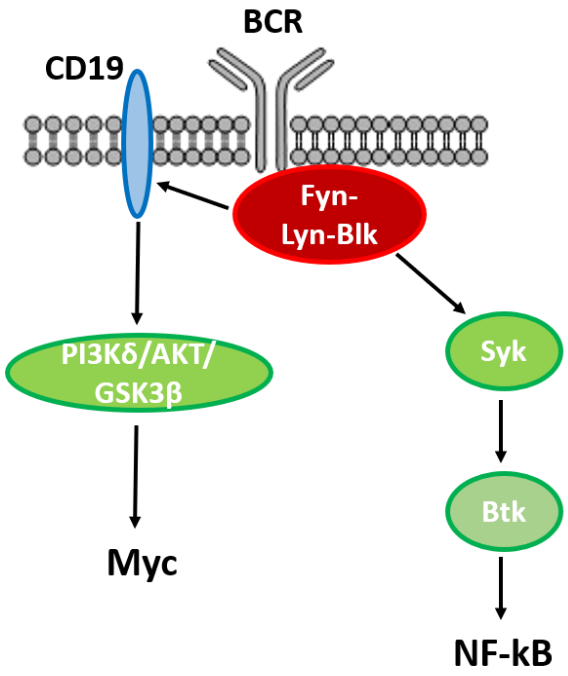

Fig. 1. BCR signaling representation.

members Lyn, Fyn and Blk with the multitarget SFK inhibitor masitinib leads to the complete block of BCR oncogenic signals in GCB- and ABC-DLBCL cells [10]. This inhibition was found to be effective on lymphoma cells and patient-derived xenograft models, which substantiates the importance of the simultaneous blockage of these SFK members in the treatment of DLBCL, as well as other forms of aggressive B-cell lymphomas [10].

Similar data have been reported by Scuoppo *et al.* who showed that the SFK inhibitor dasatinib, thanks to the suppression of Fyn activity, possesses anti-tumor activity in both ABC- and GCB-DLBCL cell lines [11]. Dasatinib resulted more active in ABC cell lines than in GCB-DLBC cells, while two other SFK inhibitors (i.e. ponatinib and saracatinib) showed similar activity on both the cell subtypes [12].

A central role for SFKs has also been shown in T-cells. Palomero *et al.* identified activating mutations of Fyn in PTCL and demonstrated that the treatment of transformed Rat1A cells expressing the Fyn Tyr531His mutant with dasatinib reduces cell growth, suggesting Fyn as a

candidate target for PTCL treatment [13]. Furthermore, Krejsgaard *et al.* reported on the involvement of Blk in CTCL [14], and have further corroborated these results by showing that dasatinib inhibits CTCL proliferation *in vitro* and *in vivo* [15]. Moreover, the pharmacological inhibition of SFKs also represents a way to overcome mechanisms of resistance to signaling inhibitors currently in clinical use, such as the BTK inhibitor ibrutinib [10,11].

Our research group is extensively involved in the development of pyrazolo[3,4-*d*]pyrimidine derivatives as SFK inhibitors [16–19]. Among them, compound Si308 (Figure 2A) has recently shown a noticeable inhibitory effect against Fyn, as well as a promising inhibitory activity in a preliminary assay on Lyn and Blk. Specifically, treatment with Si308 at a concentration of 10 μM reduces the kinase activity of Lyn and Blk by 85% and 81%, respectively [17].

In the present work, the action of Si308 on Lyn and Blk is further investigated and elucidated by means of molecular modelling studies and enzymatic evaluations. Since compound Si308 emerged as a candidate multitarget SFK inhibitor, a small library of pyrazolo[3,4-*d*]pyrimidines structurally related to Si308 was designed and docked into the ATP binding site of Fyn, Lyn and Blk. Finally, the library was synthesized and tested for anti-tumor activity in human cell lines derived from DLBCL, PTCL and CTCL. An evaluation of *in vitro* ADME properties (PAMPA permeation, water solubility, and metabolic stability) was also performed.

Overall, our efforts highlighted a number of new pyrazolo[3,4-*d*]pyrimidines endowed with good anti-tumor activity against lymphoma cells. In particular, compound **2h** proved to be a powerful multitarget inhibitor of Fyn, Lyn and Blk with remarkable antiproliferative effects on human B- and T- cell lymphoma cell lines.

2 RESULTS

2.1 Molecular modelling and enzymatic activity of the first generation compound Si308

In the present work, docking studies were carried out using Glide software [20] with the aim of understanding the possible binding mode of Si308 to SFKs. The reliability of the program was verified by docking compound **1a** (Figure 2A), a structural precursor of Si308, in the ATP binding site of the crystallographic structure of Fyn coded by PDB ID: 2DQT [21]. Results showed that the binding mode of compound **1a** within the catalytic domain of Fyn is highly comparable to that previously published [17] (Figure 2B). It is worth noting that compound **1a**, as well as most of the pyrazolo[3,4-*d*]pyrimidine derivatives studied in this work, has a chiral centre. Nevertheless, docking calculations were carried out with the R enantiomer, because in a previous crystallographic study we obtained the complex of this enantiomer with the ATP-binding site of the kinase c-Src, a SFK member [18]. However, the same study clearly showed that both enantiomers have comparable efficacy against the recombinant protein.

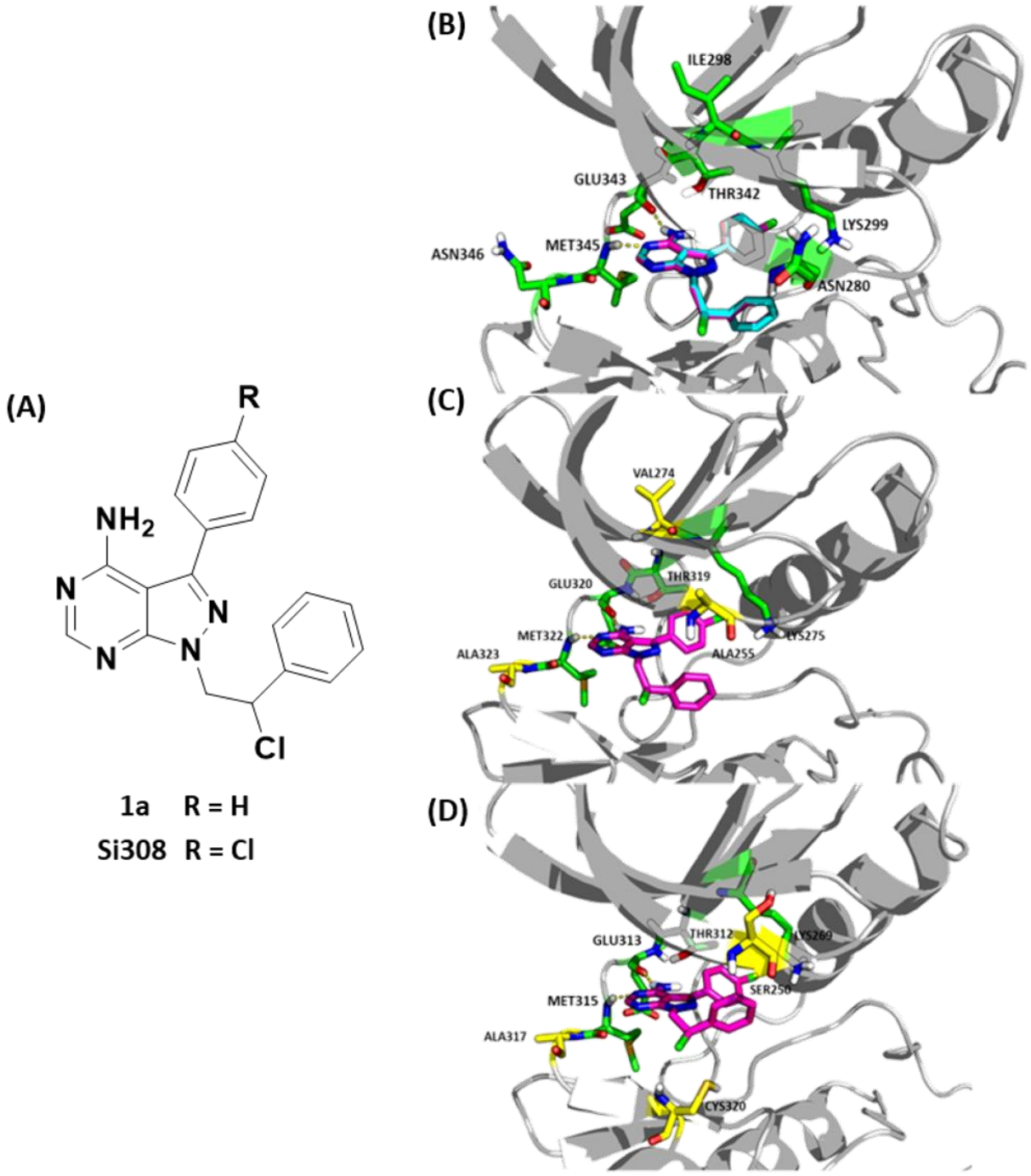

Fig. 2. Chemical structures of compounds **1a** and Si308 are reported (A). Predicted binding mode of compound Si308 and **1a** in the ATP binding pocket of Fyn (B), Lyn (C), and Blk (D). Ligands are shown as magenta and cyan sticks respectively. Ligand/protein polar contacts are highlighted by yellow dashed lines. The amino acids in yellow sticks in (C) and (D) represent the residues of the ATP binding site of Lyn and Blk that differ from Fyn.

The docking protocol was then used to dock Si308 in the ATP binding site of Fyn, Lyn and Blk that share a very high percentage of identity within the catalytic domain (Figure 3). Notably, residues of the ATP binding sites are highly conserved, which led us to hypothesize that the binding mode of Si308 could be highly comparable in the three selected targets.

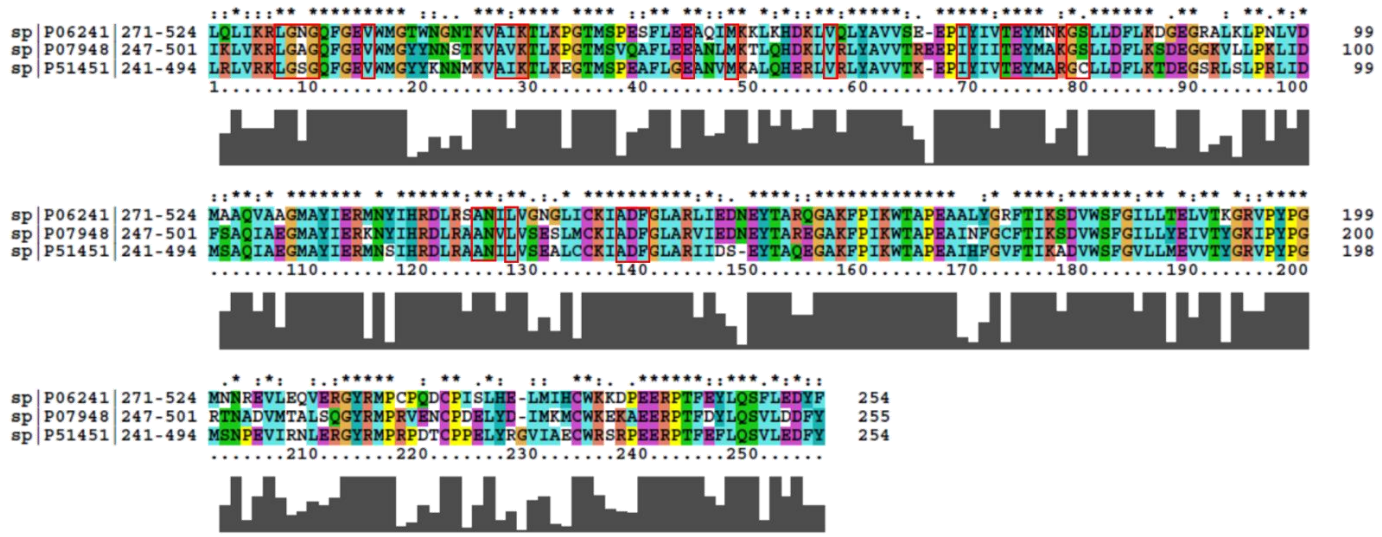

Fig. 3. Sequence alignment of the catalytic domain of Fyn, Blk and Lyn (UniProtKB codes: P06241, P51451 and P07948, respectively). Bars below the sequence alignment correspond to the degree of amino acid conservation among the sequences (full bar: residues identity; empty bar: completely different residues). The red boxes show the residues of the ATP binding site.

The X-ray crystal structure of human Lyn kinase (PDB ID: 5XY1 [22]) was selected for docking studies because of its highest resolution among available Lyn structures. In contrast, and to the best of our knowledge, the 3D structure of the catalytic domain of Blk was not available in structural databases at the time of this study. Thus, to carry out the structure-based computational analysis, it was generated by homology modelling. To this aim, a BLAST search in the Protein Data Bank (PDB) provided the human tyrosine kinase Hck as the sequence with the highest percentage of identity (75%) with respect to the query, i.e. kinase domain of Blk. Among the structures of human Hck available in the PDB, the crystallographic structure coded by PDB-ID 2HK5 was selected as template for the construction of the homology model with the Prime software [23,24] because it is in a DFG-in conformation. The preliminary homology model was first refined through the serial loop sampling approach, while the default sampling algorithm was used to adjust the conformation of side chains that do not derive from the template. The resulting model was finally relaxed through energy minimization, and its quality was assessed by the analysis of Ramachandran plots as well as by the ProSA-web tool [25,26].

As anticipated above, Si308 keeps the same binding mode in Fyn, Lyn and Blk (Figure 2) because of the high percentage of sequence identity among these proteins. Overall, the aromatic amine of Si308 establishes H-bonds with the backbone of the glutamate and the methionine of the hinge region, while the C3 phenyl group fits into the ATP binding site hydrophobic region.

To evaluate the conformational stability of Si308 in complex with Fyn, Lyn and Blk and to gain further insights into the ligand-protein interactions, molecular dynamics (MD) simulations were carried out with Amber16 on docking complexes. In particular, binding poses described in Figure 2 were solvated in a rectilinear box of explicit water molecules and counter-ions up to charge

neutralization, and relaxed through energy minimization. Following heating to 300 K and density equilibration, unrestrained MD trajectories were produced for a total of 50 ns on each complex.

Figure 4A describes the evolution of the root-mean-square deviation (RMSD) calculated on all heavy atoms of the complexes during MD simulation time with respect to the last frame of the minimization, while the RMSD of the ligand with respect to the starting poses in each complex is shown in Figure 4B. In all systems, we observed a slight initial increase of the RMSD that is followed by a stabilization at values around 2 Å after few ns, which suggests that the binding mode of Si308 is stable for the entire MD simulation time.

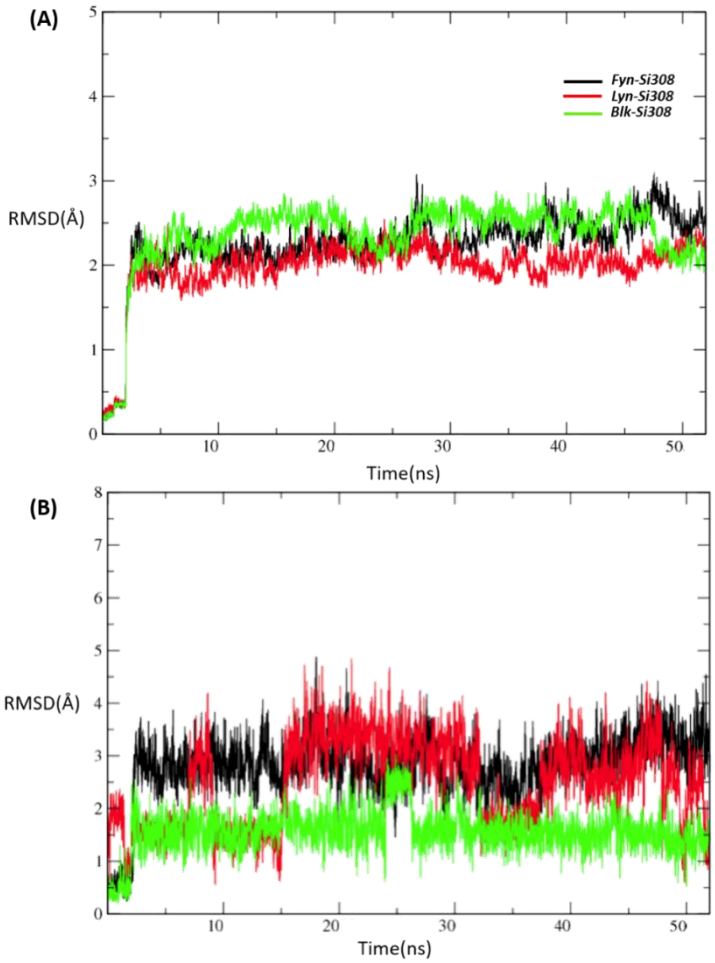

Fig. 4. (A) RMSD of the heavy atoms of the complexes (B) RMSD of the ligand in the three complexes.

Visual inspection of MD trajectories showed that Si308 is stabilized by a number of interactions within the ATP binding site of Fyn, Lyn and Blk that were further highlighted by using the pairwise decomposition of the delta energy of binding as implemented in the MM-GBSA approach (Table 1).

Table 1

Hot spots in ligand-protein interaction identified by MD simulations.

Residue in Fyn(Lyn,Blk)	delta energy of binding [Kcalmol^{-1}]		
	Si308/Fyn	Si308/Lyn	Si308/Blk
Val285(*261,**255)	-2.903	-2.861	-3.485
Ala297(*273,**267)	-2.245	-1.810	-1.836
Lys299(*275,**269)	-3.375	-3.116	-3.869
Glu314(*290,**284)	-0.304	-0.054	-0.599
Met318(*294,**288)	-0.583	-0.634	-0.533
Val327(*303,**297)	-1.201	-1.276	-0.942
Thr342(*319,**312)	-2.379	-2.221	-2.254
Glu343(*320,**313)	-3.200	-3.304	-3.050
Tyr344(*321,**314)	-3.359	-3.175	-2.887
Met345(*322,**315)	-3.694	3.736	-3.900
Leu397(*374,**367)	-3.475	-4.919	-3.582
Ala407(*384,**377)	-0.586	-2.020	-0.677
Asp408(*385,**378)	-0.587	-0.859	-1.196
Phe409(*386,**379)	-0.082	-0.088	-0.116

** numbering of the same amino acid in Lyn ** numbering of the same amino acid in Blk*

Energy values related to the interactions made by the compound in the binding site of Fyn, Lyn and Blk are comparable each other. Particularly, the most energetically-relevant interactions of Si308 are established with residues of the hinge region Glu343 and Met345, with the catalytic Lys299 and with two hydrophobic residues of the binding site Val285 and Leu397. Residue numbering corresponds to Fyn sequence; the above residues in Lyn are Glu320, Met322, Lys275, Val261 and Leu374, while in Blk they are Glu313, Met315, Lys269, Val255 and Leu367.

The MM-GBSA approach was also used to compute the theoretical delta energy of binding of the complexes. Ligand theoretical affinity values are reported in Table 2, and show highly comparable theoretical affinity of Si308 in tested kinases in agreement with docking results and with the conformational stability observed in MD simulations (Figure 4).

Table 2

Delta energy of binding of the three complexes.

Complex	delta energy of binding [Kcalmol^{-1}]

Fyn-Si308	-37.55 +/- 2.59
Lyn-Si308	-37.84 +/- 2.70
Blk-Si308	-37.28 +/- 2.48

Overall, the computational results suggest that Si308 might bind Fyn, Lyn and Blk with a comparable affinity, thus behaving as a candidate multitarget inhibitor acting on the SKF members that are relevant to B- and T-cell lymphomas.

The inhibitory activity of Si308 against target SKFs was finally confirmed by enzymatic assays carried out on recombinant Fyn, Lyn and Blk. The compound shows inhibition values in the sub-micromolar range that are highly comparable each other (Table 3), and in agreement with molecular modelling results.

Table 3

Inhibitory activities of compound Si308 toward Fyn, Lyn and Blk.

	Fyn	Lyn	Blk
	K_i [µM]	K_i [µM]	K_i [µM]
Si308	0.16 ± 0.01	0.19 ± 0.04	0.19 ± 0.05

2.2 Chemistry

Encouraged by these enzymatic results, we decided to synthesize a series of twelve derivatives of Si308, **2a-l**, with the aim of discovering new compounds with anti-tumor activity in lymphoma cell lines. The C3 phenyl ring, which accommodates within the inner side of the ATP binding pocket, was differently functionalized with point modifications in -*para*, -*ortho* and -*meta* positions, with the aim of verifying whether these decorations could lead to an increase in inhibitory activity, following the trend observed for Si308 compared to its precursor **1a** in Fyn inhibition. In addition, some compounds bearing modifications at the N1 2-chloro-2-phenylethyl side chain were synthesized, in order to explore the relevance of modifications in the solvent exposed region in this family of compounds.

The synthesis of 3-susbtituted 1-(2-chloro-2-phenylethyl)-1*H*-pyrazolo[3,4-*d*]pyrimidin-4-amines **2a-f** was achieved following a route which starts with a three-component one-pot synthesis [27]. Sodium hydride was added in small batches to a solution of malononitrile in anhydrous THF precooled at 0-5 °C. After 30 min, the suitable acyl chloride was added and the solution was stirred at room temperature until the complete transformation of the acyl chloride into the corresponding enol derivative, affording compounds **3a-f** (not isolated). Then dimethylsulfate was added, and the reaction was refluxed for 3-6 h, monitoring *via* TLC the formation of the [methoxy(phenyl)methylene]malononitrile derivatives **4a-f** (not isolated). Finally, 2-hydrazino-1-phenylethanol **5** was prepared following a literature procedure [28] and added to the reaction in a THF solution. After 4 h of reflux, the crude was purified by flash chromatography, affording the

intermediates **6a-f**. The latter were heated in the presence of formamide at 190 °C for 3-4 h to obtain the pyrazolo-pyrimidines **7a-f**. Finally, the intermediates **7a-f** were reacted with thionyl chloride in anhydrous CH_2Cl_2 at room temperature for 12 h under nitrogen atmosphere to give the desired compounds **2a-f** (Scheme 1).

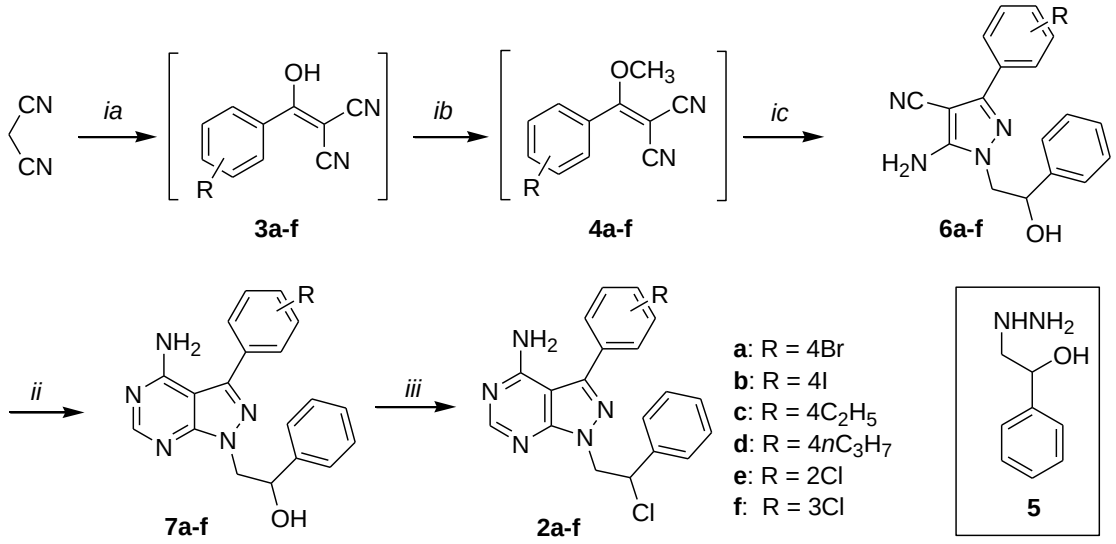

Scheme 1. Syntesis of compounds **2a-f.** *Reagents and conditions:* (*i*) a) NaH, an. THF, 0-5 °C, 30 min; then suitable acyl chloride, rt, 1.5 h; b) Me_2SO_4, reflux, 3-6 h; c) **5**, reflux, 4 h; (*ii*) formamide, 190 °C, 3-4 h; (*iii*) $SOCl_2$, an. CH_2Cl_2, rt, 12 h, N_2 atmosphere.

Synthesis of compounds **2g-l** was performed *via* a Suzuki cross-coupling route. For compound **2h** this synthetic approach was chosen since the reactivity of the primary alcohol prevented the use of the one-pot strategy. Compound **2g** was directly obtained from an intermediate of this route. For compounds **2i-l**, this approach was selected in order to introduce the variations at N1 and C3 of the pyrazolo[3,4-*d*]pyrimidine scaffold only in the last two reactions, reducing the number of steps.
In detail, for the synthesis of compounds **2g,h**, 3-iodo-1*H*-pyrazolo[3,4-*d*]pyrimidin-4-amine **8**, already prepared by us [17], was dissolved in anhydrous toluene in the presence of a solution of tetrabutylammonium fluoride (TBAF) 1 M in THF. After heating at 70 °C for 1 h, 2-bromoacetophenone was added and the reaction was stirred at 70 °C other 2 h affording 2-(4-amino-3-iodo-1*H*-pyrazolo[3,4-*d*]pyrimidin-1-yl)-1-phenylethanone **9**, which was purified by flash chromatography. The intermediate **9** was reduced by reaction with sodium borohydride in MeOH at 0 °C for 3 h giving the corresponding alcohol **10**. Then, compound **10** was reacted with $SOCl_2$ in anhydrous CH_2Cl_2 at room temperature for 12 h under nitrogen atmosphere to obtain the chlorinated derivative **11**. Finally, the Suzuki reaction between the intermediates **10** or **11** and 4-(hydroxymethyl)phenylboronic acid, in the presence of a palladium catalyst and caesium carbonate afforded the final compounds **2g** and **2h** (Scheme 2).

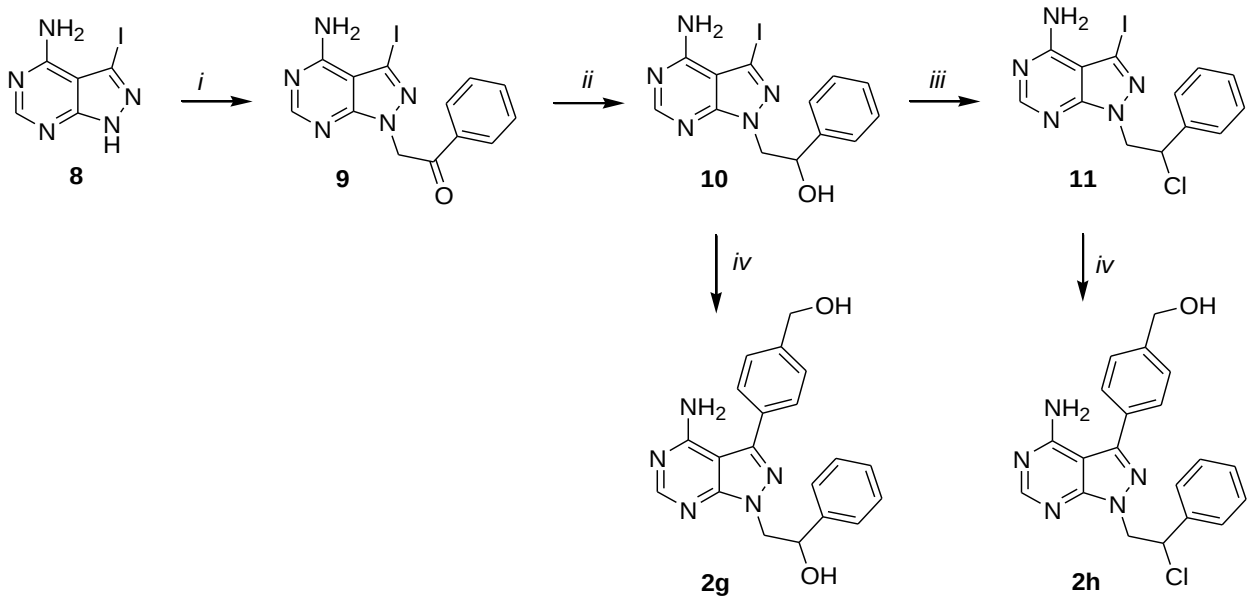

Scheme 2. Synthesis of compounds **2g,h.** *Reagents and conditions*: (*i*) TBAF 1 M in THF, an. toluene, 70 °C, 1 h; then 2-bromoacetophenone, 70 °C, 2 h; (*ii*) $NaBH_4$, MeOH, 0 °C, 3 h; (*iii*) $SOCl_2$, an. CH_2Cl_2, r.t., 12 h, N_2 atmosphere; (*iv*) 4-(hydroxymethyl)phenylboronic acid, Cs_2CO_3, Pd(dppf)Cl_2, DME, H_2O, 90 °C, 14 h.

For the synthesis of compounds **2i-l**, 3-iodo-1*H*-pyrazolo[3,4-*d*]pyrimidin-4-amine **8** was treated with 2-bromo-1-phenylpropane or (2-bromoethyl)benzene in the presence of potassium carbonate at 130 °C for 18 h, affording the 3-iodo-1*H*-pyrazolo[3,4-*d*]pyrimidin-4-amino derivatives **12a,b** [17].

Finally, compounds **12a,b** were reacted with an excess of the suitable boronic acid under Suzuki conditions to give the desired compounds **2i-l** (Scheme 3).

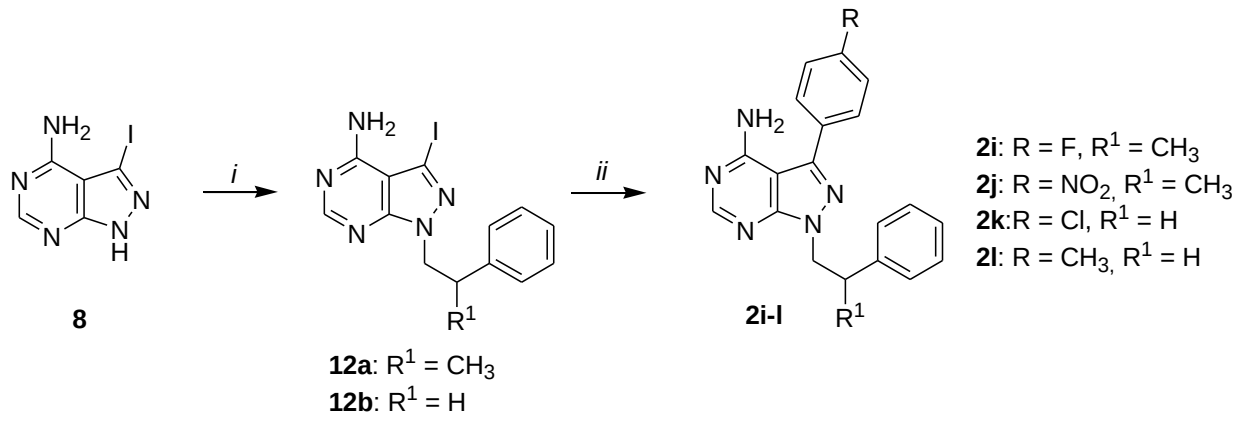

Scheme 3. Synthesis of compounds **2i-l**. *Reagents and conditions:* (*i*) 2-bromo-1-phenylpropane or (2-bromoethyl)benzene, K_2CO_3, an. DMF, 130 °C, 18 h; (*ii*) suitable boronic acid, Cs_2CO_3, Pd(dppf)Cl_2, an. toluene, 90 °C, 14 h.

2.3 Biology

The small library of compounds has been tested in tumor cell lines derived from GCB-DLBCL (n.=4; DOHH2, FARAGE, SU-DHL-8 and SU-DHL-6) and T-cell lymphoma lines (CTCL, n.=3, HUT-

78, H9 and HH; PTCL, n.=1, FE-PD). The C-3 *para*-tolyl derivative **1b**, previously reported by our research group and endowed with a promising activity towards Fyn (K_i = 95 nM) [17], has been added to the test set. We assessed the anti-proliferative activities of the compounds using the 3-(4,5-dimethylthiazol-2-yl)-2,5-diphenyltetrazolium bromide (MTT) cell viability assay, and the biological data allowed us to carry out a preliminary structure-activity relationship (SAR) evaluation on this class of derivatives.

Compound **2h** was the most potent and promising compound, with IC_{50} values lower than 10 μM in all cell lines. The compound induced slight G2/M arrest in most of the cell lines, but it was able also to induce cell death, as indicated by sub-G0 accumulation, which was more evident in the in FE-PD cells and less in HUT-78 and SU-DHL-8 (Figure 5). In term of SAR, compound **2h** had a hydroxymethyl group as C-3 substituent. Its analogue **2g**, bearing an OH instead of the chlorine atom on the N1 side chain, was slightly less active, confirming the importance of a chlorine atom on this chain.

Compound Si308 showed an IC_{50} value of 8.87 μM in the GCB-DLBCL cell line SU-DHL-8 and IC_{50} values between 11-22 μM in all the other cell lines, except for one (HUT-78), which was completely resistant. The previous generation compound **1b** was quite active on this cell line, although its activity profile results generally similar or lower than that of Si308 in the other cell lines.

Regarding the N1 side chain, the replacement of the chlorine atom with a methyl group (compounds **2i** and **2j**) or a hydrogen atom (compounds **2k** and **2l**) was generally related to an activity similar or slightly lower than that observed for the parent compound Si308. The only exception was compound **2l**, which showed an IC_{50} value of 9.74 μM in the GCB-DLBCL cell line DOHH2 cell line. It should be also noted that the introduction of a nitro group (compound **2j**) was responsible for the total loss of activity.

The displacement of the chlorine atom from the *para* position to *ortho* or *meta* positions on the C3 phenyl ring (compounds **2e** and **2f**, respectively) was also characterized by a reduction of the activity. On the other hand, the introduction of increasingly bulky substituents on the *para* position of the C3 phenyl ring (compare the 4-chloro derivative Si308 with the corresponding halogenated derivatives **2a** and **2b**, and the 4-methyl derivative **1b** with the corresponding ethyl and *n*-propyl derivatives **2c** and **2d**) did not affect the biologic activity. Indeed, the bulkier derivatives generally possess an activity similar or higher than that of the previously synthesized compounds Si308 and **1b**, but the trend was not maintained among all cell lines. Compound **2b** presented anti-proliferative activity in two cell lines (GCB-DLBCL cell line DOHH2, IC_{50} = 3.68 μM; CTCL cell line HH, IC_{50} = 5.24 μM). Compound **2d** was active in four cell lines, two derived from GCB-DLBCL cell lines (DOHH2, IC_{50} = 4.38; SU-DHL-8, IC_{50} = 6.72 μM) and two from CTCL (HUT-78, IC_{50} = 9.90; H9, IC_{50} = 4.74 μM).

Table 4

Anti-tumor activity of compounds Si308, **1b** and **2a-l** on lymphoma cell lines.

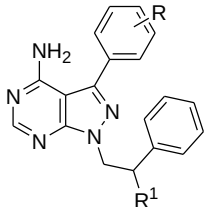

			Cell line (IC_{50}) [μM]							
			B-cell lymphoma cell line				**T-cell lymphoma cell line**			
Cpd	R	R^1	DOHH2	FARAGE	SUDHL8	SUDHL6	HUT-78	FEPD	H9	HH
Si308	4Cl	Cl	11.41	14.94	8.87	21.52	> 100	15.76	13.58	13.9
1b	$4CH_3$	Cl	11.77	19.25	12.14	23.43	11.12	> 100	> 100	14.82
2a	4Br	Cl	10.99	13.61	11.85	45.64	21.05	21.7	21.7	12.44
2b	4I	Cl	3.68	12.64	11.46	13.17	12.03	20.46	11.61	5.24
2c	$4C_2H_5$	Cl	21.18	22.74	17.47	29.68	58.00	~ 21.53	24.17	21.08
2d	$4nC_3H_7$	Cl	4.38	29.36	6.72	31.11	9.90	29.15	4.74	48.53
2e	2Cl	Cl	26.58	51.45	18.39	> 100	> 100	38.86	38.86	> 100
2f	3Cl	Cl	27.35	30.9	13.69	> 100	> 100	24.89	~22.07	43.12
2g	$4CH_2OH$	OH	12.09	26.96	27.18	34.20	> 100	26.49	~ 22.26	17.31
2h	$4CH_2OH$	Cl	2.44	7.02	6.14	9.29	4.50	10.84	3.42	2.40
2i	4F	CH_3	21.26	22.8	12.08	~ 22.92	> 100	> 100	18.76	11.81
2j	$4NO_2$	CH_3	> 100	> 100	> 100	> 100	> 100	> 100	> 100	> 100
2k	4Cl	H	11.81	18.6	35.96	> 100	> 100	31.1	> 100	18.17
2l	$4CH_3$	H	9.74	15.98	37.03	> 100	> 100	~ 21.54	> 100	17.26

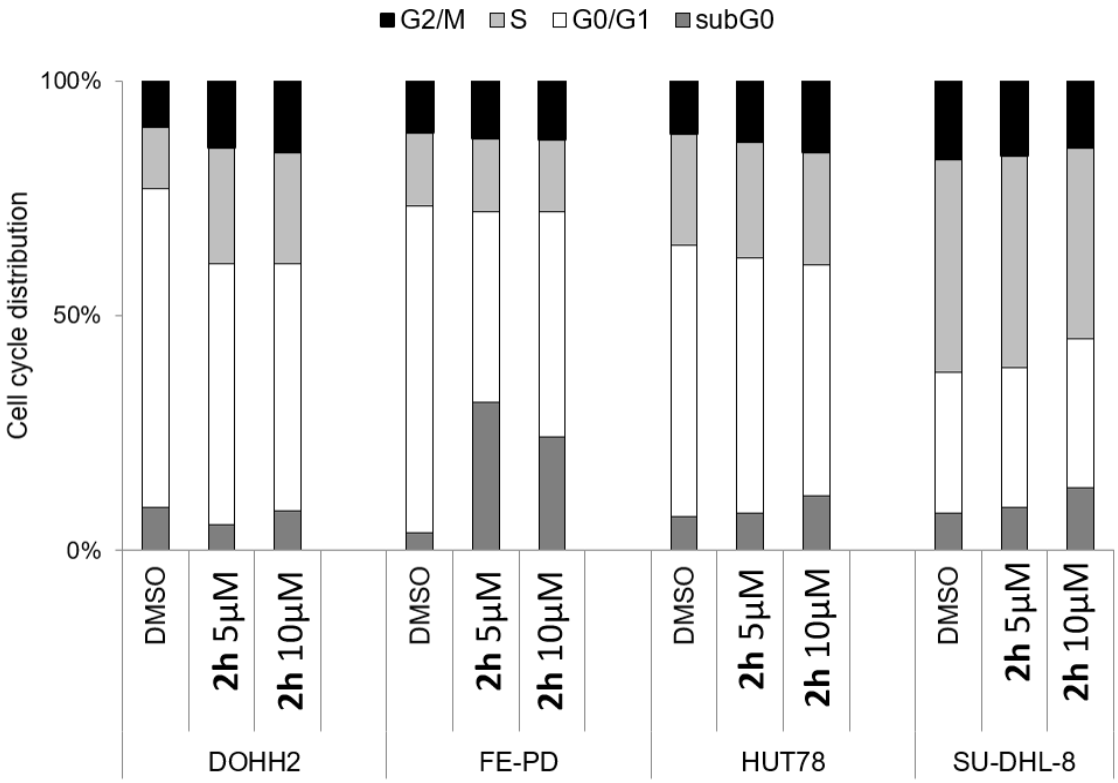

Fig. 5. Cell cycle analyses of lymphoma cell lines following treatment with compound **2h** at the concentrations of 5 and 10 μM for 72 hours. Following treatment, cells were fixed with 70% ethanol before staining with 7AAD for cell cycle analysis. The percentage of cells in each phase of the cell cycle is shown for each treatment type.

2.4 Molecular modelling and enzymatic activity of the second generation compound 2h

The possible binding mode of compound **2h** in the ATP binding site of Fyn, Lyn and Blk was investigated by molecular docking using the validated protocol described above. Overall, the compound shows a comparable binding mode in the three kinases. Similarly to Si308, compound **2h** interacts through H-bonds with the conserved glutamate and methionine residues of the hinge region, and also forms a cation-π interaction with the conserved catalytic lysine residue. In addition, compound **2h** is able to make a H-bond in all three kinases with the catalytic glutamate of the alpha c-helix, thanks to the hydroxyl group in *para* position of the ring in C3. Moreover, the same hydroxyl group is also able to make a hydrogen bond with the aspartate of the DFG motif

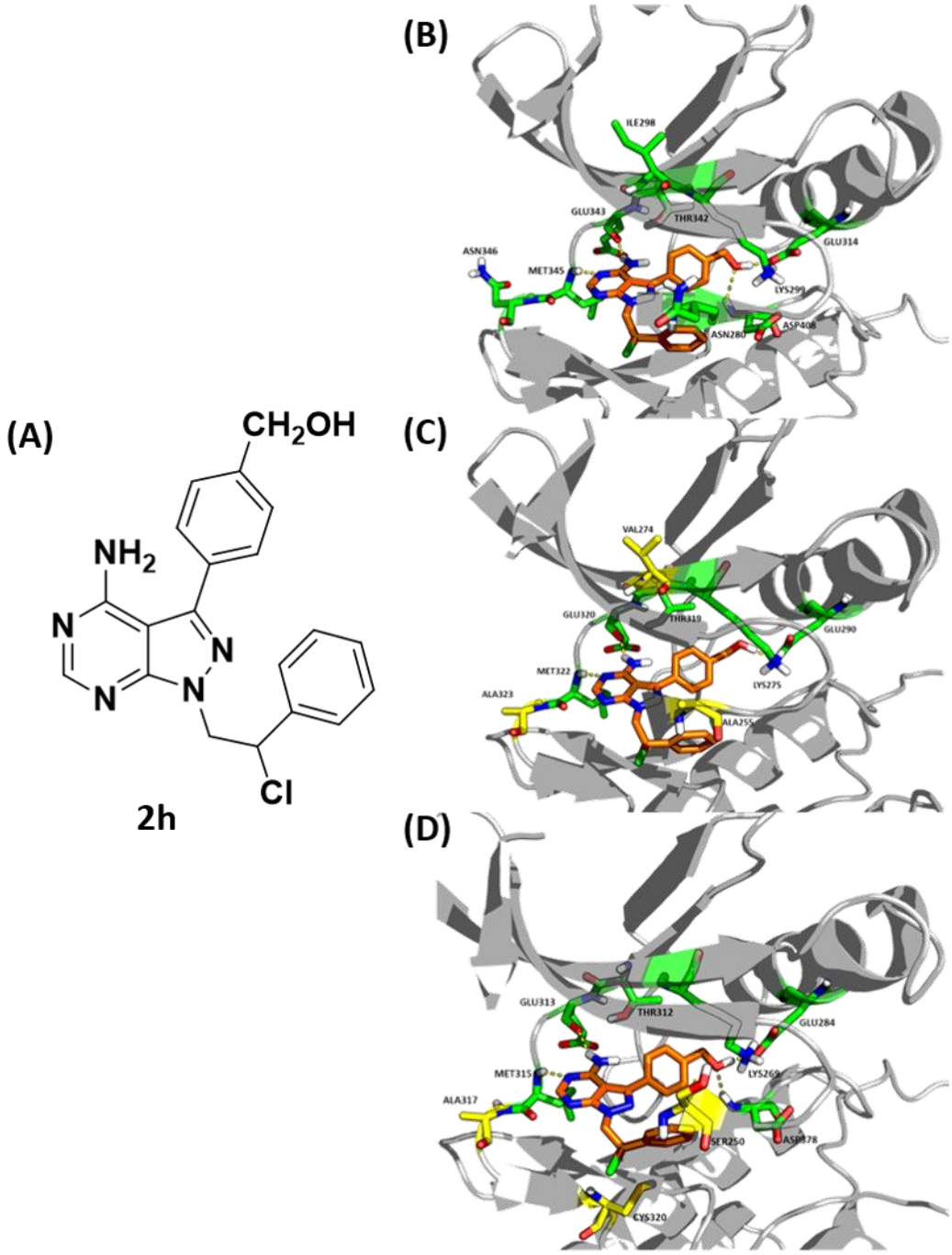

(Figure 6).

Fig. 6. Chemical structure of compound **2h** is reported (A). Predicted binding mode of compound **2h** in the ATP binding pocket of Fyn (B), Lyn (C), and Blk (D). Ligand **2h** is shown as orange sticks. Ligand/protein polar contacts are highlighted by yellow dashed lines. The amino acids in yellow sticks in (C) and (D) represent the residues of the ATP binding site of Lyn and Blk that differ from Fyn.

To further confirm the direct targeting of **2h** to Fyn, Lyn and Blk enzymatic assays were carried out showing inhibitory effects *in vitro* with K_i values in the sub-micromolar range. Notably, these values are highly comparable to those observed for the parent Si308 (see Table 3 for comparison) although Si308 showed a lower activity *in vitro* on cell lines.

Table 5

Inhibitory activities of compound **2h** toward Fyn, Lyn and Blk.

	Fyn K_i [μM]	Lyn K_i [μM]	Blk K_i [μM]
2h	0.12 ± 0.03	0.19 ± 0.02	0.17 ± 0.08

2.5 In vitro ADME studies

In vitro assays were performed to evaluate the ADME properties of the most promising compounds Si308 and **2h**, and to try to explain the different cellular profile of these molecules. In fact, **2h** proved to be ~1.5 to 5.8 fold more active than Si308 in cells even if the two compounds share a highly similar inhibitory activity against recombinant enzymes *in vitro*. Aqueous solubility and metabolic stability in the presence of human liver microsomes (HLM) were investigated, and the parallel artificial membrane permeability assay (PAMPA) towards gastrointestinal (GI) membrane was performed (Table 6).

Table 6

In vitro ADME properties of compound Si308 and **2h**.

	H_2O Sol. $\mu g \cdot mL^{-1}$ [a]	Metabolic Stab.[b,c] %	GI[b,d] P_{app} (10^{-6} $cm \cdot sec^{-1}$) %(MR)[e]
Si308	0.01	85.2	9.95 (70.4)
2h	0.09	85.0	10.80 (15.2)

[a]Determined by LC−MS-MS. Data represent mean values of at least three experiments. [b]Determined by UV/LC−MS. Data represent mean values of at least three experiments. [c]Expressed as percentage of unmodified drug. [d]Gastrointestinal parallel artificial membrane permeability assay. [e]Membrane retention (MR) expressed as percentage of compound unable to reach the acceptor compartment.

Compound **2h** possesses a water solubility of an order of magnitude higher than Si308, which is explained by the presence of a polar hydroxyl group in the molecule. Moreover, both compounds exhibit comparable metabolic stability in HLM. Regarding the passive permeability through the GI membrane, **2h** showed a slight enhancement with respect to Si308, but the most significant data is related to the different MR values. Indeed, Si308 shows a MR percentage ~5 folds higher than **2h** (70.4% vs 15.2%). Taken together, these data could explain the reasons for the higher activity of **2h** in cells compared to Si308.

3 CONCLUSIONS

Recent studies have highlighted the central role played by the three members of the SFK (Lyn, Fyn and Blk) as potential molecular targets in B-cell lymphomas [9,10,13–15]. Moreover, other studies have demonstrated the involvement of Fyn and Blk in the development of certain T-cell lymphomas [13–15]. In this work, the Fyn inhibitor Si308 was submitted to in-depth molecular modelling studies

flanked by enzyme inhibition assays to further investigate its potential as a multitarget SFK inhibitor. We confirmed that this compound is able to target Lyn and Blk with an efficacy comparable to that seen against Fyn. As a result, a small library of pyrazolo[3,4-*d*]pyrimidine derivatives related to Si308 was synthesized and tested on B- and T- lymphoma cell lines. Among the twelve synthesized derivatives, **2h** was the most potent compound, with an IC_{50} value below 10 µM against different lymphoma cell lines, and K_i values in the sub-micromolar range against the catalytic domain of recombinant Fyn, Lyn, and Blk kinases.

Compared to **2h**, compound Si308 is less active on the cell lines, despite having K_i values comparable to those of **2h**. As evidenced by *in vitro* ADME studies, this discrepancy in biological activity might be attributed to the higher percentage of Si308 that is trapped in the cell membrane compared to **2h**.

In summary, we identified a potent multitarget Fyn-Blk-Lyn inhibitor endowed with significant antiproliferative activity on different human lymphoma cell lines and a good pharmacokinetic profile. These results pave the way to further development of this class of pyrazolo[3,4-*d*]pyrimidines as promising agents for the treatment of lymphomas.

4 MATERIALS AND METHODS

4.1 Computational details

4.1.1 Protein preparation.

The crystallographic structures of Fyn and Lyn (PDB ID: 2DQT [21] and 5XY1 [22], respectively) were downloaded from the Protein Data Bank (www.rcsb.org/pdb) [29] and prepared using the Protein Preparation Wizard [30] workflow implemented in Maestro Suite Version 11.2.013. In detail, co-crystallized inhibitors and water molecules were removed, hydrogen atoms, side chains and missing loops were added using Prime [23,24], and bond orders were assigned. In addition, an optimization of the network of hydrogen bonds at pH 7.4 was carried out. Finally, the systems were refined by performing a restrained energy minimization with the OPLS3 force field that was stopped when the RMSD of the heavy atoms was below 0.30 Å.

4.1.2 Homology modelling.

The sequence of the catalytic domain of human Blk was obtained from UNIPROT database [31] (entry P51451) and used for a sequence similarity search with BLAST in the PDB.

The crystallographic structure of the human kinase domain of HCK, PDB ID: 2HK5 [32] was selected as template for the construction of the homology model by the software Prime [23,24] implemented in Maestro Suite [33]. The loop refinement task was run, using the serial loop sampling approach and choosing respectively “Default” as level of accuracy (recommended for loop length up to 5 residues). In addition, the side chain conformation of residues that do not derive from the template was refined using the "Default" sampling algorithm. Finally, the system was energy minimized with the OPLS3 force field until the RMSD of the heavy atoms was below 0.30 Å.

Model evaluation was performed through the analysis of Ramachandran plots (see Supplementary materials, Figure S1). Moreover, the reliability of the model was verified using the tool ProSA-web [25,26], which uses knowledge based potentials of mean force to evaluate the energy of the model. In particular, the z-score obtained for the structure under consideration is a measure of the deviation of the total energy of the structure with respect an energy derived from random conformation.

In Supplementary materials Figure S2 the z-score of our model is reported in the form of a black dot together with the z-scores of all experimentally determined proteins currently available in the PDB (groups of structures from different sources are distinguished by different colours).

4.1.3 Docking studies.

Molecular docking simulations were carried out by the GLIDE software [20] (SP procedure). In detail, the prepared protein systems were used to generate the receptor grids that were centred on the corresponding crystallographic ligands. After grids preparation, compounds were drawn and energy minimized using Maestro [33] and MacroModel [34], respectively. Finally, molecules were docked, treating the proteins as rigid using the default values.

4.1.4 Molecular dynamics (MD).

Maestro 11 [33] was initially used to remove all hydrogens atom from the structures provided by the Protein Preparation Wizard and homology modelling, to cap the N and C terminal residues of the protein, and to extract the ligand from the binding site.

Antechamber [35] was used to assign atomic partial charges (AM1-BCC method) and atom types to the ligands, while Parmchk2 was used to write the force field modification (frcmod) files containing any force field parameters that are needed for the molecules but not supplied by Generalized Amber Force Field (GAFF) [36] that was used to assign parameters to the ligands.

The parametrization of the proteins was performed by means of the leap module of Amber16 using the ff14SB force field [37]. Hydrogen atoms were added to each complex, before solvation in a TIP3P cuboid water box having a distance between the walls and the protein of 20 Å. An appropriate number of counterions was added to neutralize the systems.

Before MD simulations, two steps of energy minimization were performed to remove bad contacts and to relax the solvated complexes. First, the complex was kept fixed with a positional restraint weight of 100 kcal/mol·Å^2, allowing in this way the minimization of water molecules. 5000 steps of energy minimization were run, of which the first 3000 with the steepest descent algorithm and the last part with the conjugate gradient algorithm. Then, the entire system was energy minimized using 10000 steps in which the first 7000 used the steepest descent algorithm and the last the conjugate gradient algorithm.

MD with periodic boundary conditions at constant volume were run for 500 ps to heat the solvated system to 300 K, using positional restrains with a weight of 2 kcal/mol·Å^2 on the protein to prevent too large fluctuations during the heating step.

To achieve density equilibration, 1.5 ns of MD with periodic boundaries conditions at constant pressure were performed at 300 K (by using the Berendsen barostat and the Langevin thermostat to maintain the pressure and the temperature of our system constant) in two steps, the first of 500 ps and the second of 1000 ps. Also during these steps, positional restrains with a decreasing weight of 2 kcal/mol and 0.5 kcal/mol·Å^2 were used on the protein. Finally, 50 ns of unrestrained MD simulation were run at constant temperature (300 K) and constant pressure (1 atm).

During MD simulations, bonds containing hydrogen atoms were restrained with the SHAKE algorithm, and 2 fs time step was used. The electrostatic interactions were calculated using the PME (Particle Mesh Ewald) method with a cutoff of 10 Å for nonbonded interactions.

The module cpptraj implemented in Amber16 was used to analyse trajectories.

4.1.5 MM-GBSA Analysis.

This method combining molecular mechanics calculations and continuum solvation models is used to evaluate binding free energy but also to perform free energy decomposition into contributions originating from different group of atoms [38].

In principle, the calculation of the binding free energy require three independent MD simulations (for the complex, protein, and ligand separately), but typically is used the approximation that no significant conformational changes occur upon binding [39], so we used only the simulations of the complexes to obtain the snapshots for the other 2 species that are necessary for the calculation (single trajectory approach).

For all the complexes 200 snapshots were used for the calculation. How is generally made when only a comparison of states of similar entropy is desired, we did not perform the calculation of the entropy term being computationally expensive and having a large margin of error; therefore, the energy values produced in the work are attributable to ΔH_{bin}.

The MM-GBSA approach was also used to perform a pairwise energy decomposition in order to map the interactions within the binding site that have a dominant role in the stabilization of the complexes.

4.2 Chemistry

All commercially available chemicals and solvents were used as purchased (Merck-Sigma Aldrich, Milan, Italy, or Alfa-Aesar, Karlsruhe, Germany). Anhydrous toluene was dried over sodium and benzophenone as an indicator; anhydrous THF was obtained by passing the solvent over a column of neutral alumina followed by storage over 3 Å molecular sieves; anhydrous CH_2Cl_2 and anhydrous dimethylformamide (DMF) were used as purchased. Chromatographic separations were performed on columns packed with silica gel 220-440 mesh, 60 Å, for flash technique, or silica gel 0.060-0.200 mm, 40 Å. TLC (thin layer chromatography) was carried out using Merck TLC plates silica gel 60 F254. Melting points (Mp) were determined with a Büchi B-540 apparatus and are uncorrected. ^{1}H NMR and ^{13}C NMR spectra were recorded on a Bruker AC200F spectrometer (at 400

MHz for ^{1}H and 100 MHz for ^{13}C) or on a Varian Gemini 200 (at 200 MHz for ^{1}H and 50 MHz for ^{13}C). Chemical shifts (δ scale) are reported in parts per million (ppm) with reference to solvent residues in DMSO-d6 (2.50 ppm for proton and 39.52 ppm for carbon), $CDCl_3$ (7.26 ppm for proton and 77.16 ppm for carbon). Data are shown as following: chemical shift, multiplicity (s = singlet, d = doublet, t = triplet, q = quartet, sx = sextet, m = multiplet, br s = broad singlet), coupling constant (*J*) in Hertz (Hz) and integration. Mass spectra (MS) were acquired using an Agilent 1100 LC-MSD VL system (G1946C) by direct injection with a 0.4 mL/min flow rate using a binary solvent system of 95/5 CH_3OH/ H_2O. UV detection was monitored at 254 nm. Mass spectra were acquired in positive mode scanning over the mass range 105-1500 m/z, using a variable fragmentor voltage of 10-70 mV. IR spectra were measured in KBr with a Perkin-Elmer 398 spectrophotometer. Elemental analysis for C, H and N was determined using Thermo Scientific Flash 2000 and results were within ±0.4% of the theoretical value. All target compounds possessed a purity of ≥95% as verified by elemental analyses by comparison with the theoretical values.
Compounds Si308, **1b**, **8** and **12a** have been already reported by us [17].

*4.2.1 General procedure for the synthesis of derivatives **6a-f**.*
A 60% sodium hydride dispersion in mineral oil (1.21 g, 30.3 mmol) was added in small batches to a solution of malonitrile (1.00 g, 15.1 mmol) in anhydrous THF (25 mL) precooled at 0-5 °C. After 30 min at 0-5 °C, the suitable acyl chloride (15.1 mmol) was added dropwise. The orange solution was stirred at room temperature for 1.5 h, until the complete transformation of the acyl chloride to the corresponding enol derivative (not isolated intermediates **3a-f**). Then dimethylsulfate (1.75 mL, 18.2 mmol) was added dropwise and the solution was refluxed for 3-6 h, monitoring *via* TLC the formation of the methoxy(phenyl)methylene]malononitrile derivatives **4a-f** (not isolated). Finally, 2-hydrazino-1-phenylethanol **5** (4.62 g, 30.2 mmol) dissolved in anhydrous THF (2 mL) was added and the reaction was refluxed for 4 h. After cooling to room temperature, water (25 mL) and conc NH_3 (5 mL) were added under stirring. After 15 min, THF was removed under reduced pressure and the aqueous phase was extracted with CH_2Cl_2 (3 × 30 mL). Organic phases were washed with water (15 mL) and brine (15 mL), dried (Na_2SO_4), and evaporated under reduced pressure. The crudes were purified by flash chromatography (silica gel 0.060-0.200 mm, 40 Å) using a proper gradient elution from petroleum ether (PE) (bp 40-60 °C)/Et_2O (8:2) to Et_2O to afford compounds **6a-f**.
4.2.1.1 *5-Amino-3-(4-bromophenyl)-1-(2-hydroxy-2-phenylethyl)-1H-pyrazole-4-carbonitrile (**6a**).* **Yield**: 41%. White solid. **Mp**: 186-188 °C. **^{1}H NMR** (400 MHz, $CDCl_3$): δ (ppm) 7.76-7.74 (m, 2H), 7.54-7.53 (m, 2H), 7.40-7.37 (m, 5H), 5.19-5.17 (m, 1H), 4.79 (br s, 1H), 4.27-4.24 (m, 1H), 4.13-4.07 (m, 1H). **^{13}C NMR** (100 MHz, $CDCl_3$): δ (ppm) 182.93, 153.29, 149.54, 140.06, 132.11, 130.89, 129.09, 128.84, 127.95, 125.94, 123.73, 115.22, 74.63, 55.85. **IR** (KBr) cm^{-1}: 3500-3300 (OH), 3398, 3329 (NH_2), 2194 (CN). **MS** (ESI): *m/z* = 382.9 $[M]^+$. **Anal. calcd.** for $C_{18}H_{15}N_4OBr$: C

56.41, H 3.95, N 14.62; **found**: C 56.52, H 4.01, N 14.25.

4.2.1.2 5-*Amino-1-(2-hydroxy-2-phenylethyl)-3-(4-iodophenyl)-1H-pyrazole-4-carbonitrile* ***(6b)***. **Yield**: 41%. White solid. **Mp**: 173-177 °C. **^{1}H NMR** (200 MHz, $CDCl_3$): δ (ppm) 7.81-7.77 (m, 2H), 7.67-7.63 (m, 2H), 7.44-7.40 (m, 5H), 5.23-5.19 (m, 1H), 4.37-4.06 (m, 2H). **^{13}C NMR** (50 MHz, $CDCl_3$): δ (ppm) 180.87, 152.91, 152.00, 138.81, 137.83, 133.25, 128.92, 128.58, 127.89, 125.94, 115.54, 96.77, 72.51, 50.23. **IR** (KBr) cm^{-1}: 3500-2800 (OH), 3398, 3329 (NH_2), 2195 (CN). **MS** (ESI): *m/z* = 431.7 $[M+H]^+$. **Anal. calcd.** for $C_{18}H_{15}N_4OI$: C 50.25, H 3.51, N 13.02; **found**: C 50.55, H 3.56, N 13.30.

4.2.1.3 *5-Amino-3-(4-ethylphenyl)-1-(2-hydroxy-2-phenylethyl)-1H-pyrazole-4-carbonitrile* ***(6c)***. **Yield**: 44%. White solid. **Mp**: 161-164 °C. **^{1}H NMR** (200 MHz, $CDCl_3$): δ (ppm) 7.84-7.81 (m, 2H), 7.44-7.40 (m, 5H), 7.30-7.27 (m, 2H), 5.13-5.09 (m, 1H), 4.67 (br s, 2H), 4.16-4.03 (m, 2H), 2.71 (q, *J* = 7.4 Hz, 2H), 1.28 (t, *J* = 7.4 Hz, 3H). **^{13}C NMR** (50 MHz, $CDCl_3$): δ (ppm) 152.91, 152.05, 146.89, 138.88, 133.23, 129.40, 128.93, 128.54, 125.96, 125.21, 123.62, 115.54, 72.56, 50.28, 40.11, 28.55. **IR** (KBr) cm^{-1}: 3500-2800 (OH), 3393, 3320 (NH_2), 2216 (CN). **MS** (ESI): *m/z* = 333.1 $[M+H]^+$. **Anal. calcd.** for $C_{20}H_{20}N_4O$: C 72.27, H 6.06, N 16.86; **found**: C 72.14, H 6.14, N 16.55.

4.2.1.4 *5-Amino-1-(2-hydroxy-2-phenylethyl)-3-(4-propylphenyl)-1H-pyrazole-4-carbonitrile* ***(6d)***. **Yield**: 48%. White solid. **Mp**: 107-109 °C. **^{1}H NMR** (200 MHz, $CDCl_3$): δ (ppm) 7.83-7.80 (m, 2H), 7.43-7.29 (m, 5H), 7.29-7.24 (m, 2H), 5.28-5.22 (m, 1H), 4.30-4.29 (m, 1H), 4.17-4.12 (m, 1H), 2.64 (t, *J* = 7.2 Hz, 2H), 1.68 (sx, *J* = 7.2 Hz, 2H), 0.97 (t, *J* = 7.2 Hz, 3H). **^{13}C NMR** (50 MHz, $CDCl_3$): δ (ppm) 152.91, 152.03, 151.47, 138.80, 133.23, 129.45, 128.96, 128.56, 125.99, 125.21, 122.98, 115.54, 72.54, 50.92, 37.61, 24.70, 12.43. **IR** (KBr) cm^{-1}: 3500-2800 (OH), 3392, 3324 (NH_2), 2217 (CN). **MS** (ESI): *m/z* = 347.3 $[M+H]^+$. **Anal. calcd.** for $C_{21}H_{22}N_4O$: C 72.81, H 6.40, N 16.17; **found**: C 72.68, H 6.72, N 16.45.

4.2.1.5 *5-Amino-3-(2-chlorophenyl)-1-(2-hydroxy-2-phenylethyl)-1H-pyrazole-4-carbonitrile* ***(6e)***. **Yield**: 37%. White solid. **Mp**: 131-134 °C. **^{1}H NMR** (200 MHz, $CDCl_3$): δ (ppm) 7.48-7.29 (m, 9H), 5.19-5.16 (m, 1H), 4.20-4.11 (m, 2H). **^{13}C NMR** (50 MHz, $CDCl_3$): δ (ppm) 151.27, 148.70, 139.07, 132.20, 130.27, 129.43, 129.18, 128.32, 127.87, 127.62, 125.82, 125.16, 124.73, 113.47, 73.36, 54.70. **IR** (KBr) cm^{-1}: 3450-2800 (OH), 3426, 3327 (NH_2), 2218 (CN). **MS** (ESI): *m/z* = 339.8 $[M+H]^+$. **Anal. calcd.** for $C_{18}H_{15}N_4OCl$: C 63.81, H 4.46, N 16.54; **found**: C 63.88, H 4.72, N 16.38.

4.2.1.6 *5-Amino-3-(3-chlorophenyl)-1-(2-hydroxy-2-phenylethyl)-1H-pyrazole-4-carbonitrile* ***(6f)***. **Yield**: 39%. White solid. **Mp**: 172-180 °C. **^{1}H NMR** (200 MHz, $CDCl_3$): δ (ppm) 7.46-7.27 (m, 9H), 5.16-5.12 (m, 1H), 4.21-4.09 (m, 2H). **^{13}C NMR** (50 MHz, $CDCl_3$): δ (ppm) 151.12, 147.89, 139.17, 132.65, 130.65, 129.55, 129.35, 128.10, 127.91, 127.82, 125.54, 125.19, 124.18, 113.51, 73.44, 55.81. **IR** (KBr) cm^{-1}: 3450-2900 (OH), 3407, 3327 (NH_2), 2218 (CN). **MS** (ESI): *m/z* = 339.7 $[M+H]^+$. **Anal. calcd.** for $C_{18}H_{15}N_4OCl$: C 63.81, H 4.46, N 16.54; **found**: C 63.86, H 4.56, N 16.83.

4.2.2 General procedure for the synthesis of derivatives ***7a-f****.*

A suspension of the suitable intermediate **6a-d** (3 mmol) in formamide (18 mL, 450 mmol) was

heated at 190 °C for 3-4 h and then poured into water (40 mL). The crude solid was filtered, washed with water, suspended in ethanol, and boiled with charcoal for 10 min. The solid dissolved at the ethanol boiling point. After charcoal filtration, compounds **7a-f** precipitated as pure solids.

4.2.2.1 *2-[4-Amino-3-(4-bromophenyl)-1H-pyrazolo[3,4-d]pyrimidin-1-yl]-1-phenylethanol (**7a**).* **Yield**: 65%. White solid. **Mp**: 198-201 °C. **^{1}H NMR** (400 MHz, $CDCl_3$): δ (ppm) 8.28 (s, 1H), 7.73-7.71 (m, 2H), 7.55-7.51 (m, 2H), 7.45-7.29 (m, 5H), 5.32-5.31 (m, 1H), 4.76-4.60 (m, 2H). **^{13}C NMR** (100 MHz, $CDCl_3$): 152.96, 147.21, 145.77, 140.25, 133.42, 131.50, 130.54, 129.83, 128.87, 127.07, 125.99, 125.15, 97.10, 73.00, 55.14. **IR** (KBr) cm^{-1}: 3500-2900 (OH), 3406, 3293 (NH_2). **MS** (ESI): *m/z* = 411.9 $[M+H]^+$. **Anal. calcd.** for $C_{19}H_{16}N_5OBr$: C 55.62, H 3.95, N 17.07; **found**: C 55.81, H 4.06, N 16.74.

4.2.2.2 *2-[4-Amino-3-(4-iodophenyl)-1H-pyrazolo[3,4-d]pyrimidin-1-yl]-1-phenylethanol (**7b**).* **Yield**: 44%. White solid. **Mp**: 218-220 °C. **^{1}H NMR** (200 MHz, $CDCl_3$): δ (ppm) 8.32 (s, 1H), 8.00-7.81 (m, 4H), 7.46-7.29 (m, 5H), 5.40-5.23 (m, 1H), 4.87-4.56 (m, 2H). **^{13}C NMR** (50 MHz, $CDCl_3$): 159.51, 153.86, 153.45, 153.07, 138.89, 137.84, 132.61, 130.77, 128.92, 128.56, 127.83, 125.91, 96.72, 71.60, 54.28. **IR** (KBr) cm^{-1}: 3500-2900 (OH), 3408, 3294 (NH_2). **MS** (ESI): *m/z* = 458.6 $[M+H]^+$. **Anal. calcd.** for $C_{19}H_{16}N_5OI$: C 49.91, H 3.53, N 15.32; **found**: C 50.13, H 3.53, N 15.27.

4.2.2.3 *2-[4-Amino-3-(4-ethylphenyl)-1H-pyrazolo[3,4-d]pyrimidin-1-yl]-1-phenylethanol (**7c**).* **Yield**: 60%. White solid. **Mp**: 54-59 °C. **^{1}H NMR** (400 MHz, DMSO-d6): δ (ppm) 8.19 (s, 1H), 7.55-7.53 (m, 2H), 7.37-7.20 (m, 7H), 5.56 (br s, 1H), 5.16-5.14 (m, 1H), 4.53-4.48 (m, 1H), 4.36-4.31 (m, 1H), 2.66 (q, *J* = 7.6 Hz, 2H), 1.22 (t, *J* = 7.6 Hz, 3H). **^{13}C NMR** (100 MHz, DMSO-d6): 158.71, 156.32, 154.92, 147.30, 144.81, 144.10, 143.61, 130.90, 128.75, 128.04, 127.91, 126.59, 97.82, 71.93, 54.18, 28.53, 16.06. **IR** (KBr) cm^{-1}: 3600-2800 (OH), 3468, 3303 (NH_2). **MS** (ESI): *m/z* = 360.3 $[M+H]^+$. **Anal. calcd.** for $C_{21}H_{21}N_5O$: C 70.17, H 5.89, N 19.48; **found**: C 70.05, H 6.18, N 19.77.

4.2.2.4 *2-[4-Amino-3-(4-propylphenyl)-1H-pyrazolo[3,4-d]pyrimidin-1-yl]-1-phenylethanol (**7d**).* **Yield**: 45%. White solid. **Mp**: 57-58 °C. **^{1}H NMR** (400 MHz, $CDCl_3$): δ (ppm) 8.28 (s, 1H), 7.56-7.54 (m, 2H), 7.46-7.44 (m, 2H), 7.37-7.29 (m, 5H), 5.30-5.27 (m, 1H), 4.92 (br s, 1H), 4.70-4.65 (m, 2H), 2.66 (t, *J* = 7.6 Hz, 2H), 1.68 (sx, *J* = 7.6 Hz, 2H), 0.97 (t, *J* = 7.6 Hz, 3H). **^{13}C NMR** (100 MHz, $CDCl_3$): 155.88, 153.59, 151.04, 146.14, 145.18, 143.78, 140.60, 129.90, 129.52, 129.14, 128.69, 128.12, 126.08, 73.34, 55.27, 37.70, 24.32, 14.00. **IR** (KBr) cm^{-1}: 3400-2900 (OH), 3471, 3304 (NH_2). **MS** (ESI): *m/z* = 374.1 $[M+H]^+$. **Anal. calcd.** for $C_{22}H_{23}N_5O$: C 70.76, H 6.21, N 18.75; **found**: C 70.62, H 6.40, N 18.64.

4.2.2.5 *2-[4-Amino-3-(2-chlorophenyl)-1H-pyrazolo[3,4-d]pyrimidin-1-yl]-1-phenylethanol (**7e**).* **Yield**: 46%. White solid. **Mp**: 126-129 °C. **^{1}H NMR** (200 MHz, $CDCl_3$): δ (ppm) 8.35 (s, 1H), 7.53-7.29 (m, 9H), 5.38-5.26 (m, 1H), 4.76-4.74 (m, 2H). **^{13}C NMR** (50 MHz, $CDCl_3$): 156.34, 154.05, 153.61, 142.38, 139.60, 134.54, 133.37, 129.68, 128.50, 127.96, 127.56, 127.06, 125.33, 124.97, 97.22, 72.26, 54.53. **IR** (KBr) cm^{-1}: 3600-2800 (OH), 3319, 3183 (NH_2). **MS** (ESI): *m/z* = 366.3

$[M+H]^+$. **Anal. calcd.** for $C_{19}H_{16}N_5OCl$: C 62.38, H 4.41, N 19.14; **found**: C 62.77, H 4.45, N 19.47.

4.2.2.6 *2-[4-Amino-3-(3-chlorophenyl)-1H-pyrazolo[3,4-d]pyrimidin-1-yl]-1-phenylethanol* ***(7f).*** **Yield**: 50%. White solid. **Mp**: 84-89 °C. **^{1}H NMR** (400 MHz, $CDCl_3$): δ (ppm) 8.30 (s, 1H), 7.68-7.60 (m, 1H), 7.52-7.30 (m, 8H), 5.31-5.28 (m, 1H), 4.95 (br s, 1H), 4.73-4.62 (m, 2H). **^{13}C NMR** (100 MHz, $CDCl_3$): 173.20, 155.62, 153.59, 151.04, 144.67, 140.60, 136.01, 133.72, 131.17, 130.15, 128.88, 128.75, 126.27, 126.08, 97.81, 73.36, 55.27. **IR** (KBr) cm^{-1}: 3550-2800 (OH), 3319, 3180 (NH_2). **MS** (ESI): *m/z* = 366.4 $[M+H]^+$. **Anal. calcd.** for $C_{19}H_{16}N_5OCl$: C 62.38, H 4.41, N 19.14; **found**: C 62.19, H 4.78, N 19.13.

4.2.3 General procedure for the synthesis of final compounds ***2a-f****.*

$SOCl_2$ (80 µL, 1.1 mmol) was added dropwise to a solution of the suitable intermediate **7a-f** (0.5 mmol) in anhydrous CH_2Cl_2 (5 mL), and the reaction was stirred at room temperature for 12 h under nitrogen atmosphere. Water (5 mL) and 1N NaOH (1 mL) were added with caution, and the aqueous phase was extracted with CH_2Cl_2 (2 × 5 mL). Then the organic phase was washed with water (5 mL) and brine (5 mL), dried (Na_2SO_4), and concentrated under reduced pressure. The crudes were purified by column chromatography (silica gel 220-440 mesh, 60 Å) using a proper mixture of CH_2Cl_2/MeOH (99:1 to obtain compounds **2a**, **2c**, **2e,f**, 98:2 to obtain compound **2d**, and 95:5 to obtain compound **2b**) as the eluent to afford compounds **2a-f**.

4.2.3.1 *3-(4-Bromophenyl)-1-(2-chloro-2-phenylethyl)-1H-pyrazolo[3,4-d]pyrimidin-4-amine* ***(2a).*** **Yield**: 42%. White solid. **Mp**: 196-199 °C. **^{1}H NMR** (200 MHz, DMSO-d6): δ (ppm) 8.26 (s, 1H), 7.75-7.71 (m, 2H), 7.61-7.53 (m, 4H), 7.38-7.36 (m, 3H), 5.88-5.68 (m, 1H), 5.12-4.92 (m, 1H), 4.89-4.74 (m, 1H). **^{13}C NMR** (50 MHz, DMSO-d6): 159.57, 153.89, 153.41, 137.44, 132.64, 131.35, 130.78, 129.67, 128.96, 128.21, 127.73, 124.01, 101.74, 59.56, 49.37. **IR** (KBr) cm^{-1}: 3455, 3307 (NH_2). **MS** (ESI): *m/z* = 429.7 $[M+H]^+$. **Anal. calcd.** for $C_{19}H_{15}N_5BrCl$: C 53.23, H 3.53, N 16.34; **found**: C 53.12, H 3.57, N 16.11.

4.2.3.2 *1-(2-Chloro-2-phenylethyl)-3-(4-iodophenyl)-1H-pyrazolo[3,4-d]pyrimidin-4-amine* ***(2b).*** **Yield**: 53%. White solid. **Mp**: 215-218 °C. **^{1}H NMR** (200 MHz, DMSO-d6): δ (ppm) 8.28 (s, 1H), 7.94-7.89 (m, 2H), 7.55-7.38 (m, 7H), 5.87-5.63 (m, 1H), 5.13-4.98 (m, 1H), 4.89-4.76 (m, 1H). **^{13}C NMR** (50 MHz, DMSO-d6): 159.43, 153.87, 153.41, 153.08, 137.85, 137.42, 132.61, 130.74, 128.91, 128.64, 127.89, 127.72, 96.72, 59.50, 49.37. **IR** (KBr) cm^{-1}: 3450, 3303 (NH_2). **MS** (ESI): *m/z* = 476.5 $[M+H]^+$. **Anal. calcd.** for $C_{19}H_{15}N_5ICl$: C 47.97, H 3.18, N 14.72; **found**: C 47.99, H 3.35, N 14.66.

4.2.3.3 *1-(2-Chloro-2-phenylethyl)-3-(4-ethylphenyl)-1H-pyrazolo[3,4-d]pyrimidin-4-amine* ***(2c).*** **Yield**: 53%. White solid. **Mp**: 228-229 °C. **^{1}H NMR** (200 MHz, DMSO-d6): δ (ppm) 8.27 (s, 1H), 7.60-7.56 (m, 3H), 7.42-7.37 (m, 6H), 5.87-5.69 (m, 1H), 5.11-4.99 (m, 1H), 4.91-4.77 (m, 1H), 2.70 (q, *J* = 7.2 Hz, 2H), 1.24 (t, *J* = 7.2 Hz, 3H). **^{13}C NMR** (50 MHz, DMSO-d6): 159.53, 153.87, 153.07, 146.81, 137.45, 132.69, 130.73, 129.45, 128.93, 128.61, 127.73, 125.21, 98.66, 72.56, 49.36, 28.52, 17.04. **IR** (KBr) cm^{-1}: 3453, 3305 (NH_2). **MS** (ESI): *m/z* = 378.7 $[M+H]^+$. **Anal. calcd.**

for $C_{21}H_{20}N_5Cl$: C 66.75, H 5.33, N 18.53; **found**: C 66.91, H 5.40, N 18.56.

4.2.3.4 *1-(2-Chloro-2-phenylethyl)-3-(4-propylphenyl)-1H-pyrazolo[3,4-d]pyrimidin-4-amine* ***(2d).*** **Yield**: 46%. White solid. **Mp**: 190-192 °C. **^{1}H NMR** (200 MHz, DMSO-d6): δ (ppm) 8.27 (s, 1H), 7.66-7.55 (m, 4H), 7.39-7.35 (m, 5H), 5.87-5.63 (m, 1H), 5.09-4.94 (m, 1H), 4.89-4.76 (m, 1H), 2.60 (t, *J* = 7.6 Hz, 2H), 1.63 (sx, *J* = 7.6 Hz, 2H), 0.93 (t, *J* = 7.6 Hz, 3H). **^{13}C NMR** (50 MHz, DMSO-d6): 159.55, 153.83, 153.42, 153.07, 151.48, 137.45, 132.65, 129.48, 128.92, 128.63, 127.74, 125.26, 98.68, 72.58, 49.48, 28.50, 17.24, 12.53. **IR** (KBr) cm^{-1}: 3454, 3303 (NH_2). **MS** (ESI): *m/z* = 392.5 $[M+H]^+$. **Anal. calcd.** for $C_{22}H_{22}N_5Cl$: C 67.42, H 5.66, N 17.87; **found**: C 67.63, H 5.36, N 17.60.

4.2.3.5 *3-(2-Chlorophenyl)-1-(2-chloro-2-phenylethyl)-1H-pyrazolo[3,4-d]pyrimidin-4-amine* ***(2e).*** **Yield**: 39%. White solid. **Mp**: 181-184 °C. **^{1}H NMR** (400 MHz, DMSO-d6): δ (ppm) 8.21 (s, 1H), 7.65-7.59 (m, 1H), 7.56-7.41 (m, 5H), 7.34-7.32 (m, 3H), 5.68-5.64 (m, 1H), 5.01-4.95 (m, 1H), 4.82-4.77 (m, 1H). **^{13}C NMR** (100 MHz, DMSO-d6): 158.25, 156.55, 154.77, 141.98, 138.43, 133.33, 132.45, 131.82, 131.44, 130.50, 129.39, 129.12, 128.07, 127.96, 99.34, 60.93, 53.07. **IR** (KBr) cm^{-1}: 3496, 3296 (NH_2). **MS** (ESI): *m/z* = 385.1 $[M+H]^+$. **Anal . calcd.** for $C_{19}H_{15}N_5Cl_2$: C 59.39, H 3.93, N 18.23; **found**: C 59.60, H 3.95, N 17.93.

4.2.3.6 *3-(3-Chlorophenyl)-1-(2-chloro-2-phenylethyl)-1H-pyrazolo[3,4-d]pyrimidin-4-amine* ***(2f).*** **Yield**: 42%. White solid. **Mp**: 162-163 °C. **^{1}H NMR** (200 MHz, DMSO-d6): δ (ppm) 8.28 (s, 1H), 7.66-7.55 (m, 6H), 7.40-7.36 (m, 3H), 5.79-5.71 (m, 1H), 5.12-4.98 (m, 1H), 4.88-4.76 (m, 1H). **^{13}C NMR** (50 MHz, DMSO-d6): 158.43, 156.66, 155.09, 142.12, 138.58, 133.43, 132.42, 131.78, 131.18, 130.56, 129.94, 129.15, 128.14, 122.28, 99.35, 61.03, 53.26. **IR** (KBr) cm^{-1}: 3473, 3294 (NH_2). **MS** (ESI): *m/z* = 385.9 $[M+H]^+$. **Anal. calcd.** for $C_{19}H_{15}N_5Cl_2$: C 59.39, H 3.93, N 18.23; **found**: C 59.54, H 4.00, N 18.46.

4.2.4 2-(4-Amino-3-iodo-1H-pyrazolo[3,4-d]pyrimidin-1-yl)-1-phenylethanone ***9.***

A solution of TBAF 1 M in THF (7.05 mL, 7.05 mmol) was added to a solution of 3-iodo-1*H*-pyrazolo[3,4-*d*]pyrimidin-4-amine **8** (1.84 g, 7.05 mmol) in anhydrous toluene (40 mL), and the mixture was heated at 70 °C for 1 h. Then, 2-bromoacetophenone (1.7 g, 8.46 mmol) was added and the reaction was stirred at 70 °C for 2 h. After cooling to room temperature, toluene was evaporated, H_2O was added and the aqueous phase was extracted with CH_2Cl_2 (3 x 50 mL). The organic phases were washed with water (3 x 50 mL), dried (Na_2SO_4), and concentrated under reduced pressure. The crude was purified by column chromatography (silica gel 220-440 mesh, 60 Å) using a gradient elution from AcOEt/n-hexane (9:1) to AcOEt/MeOH (9:1) to afford the compound **9**. **Yield**: 47%. White solid. **Mp**: 227-231 °C. **^{1}H NMR** (400 MHz, DMSO-d6): δ (ppm) 8.15 (s, 1H), 8.05-8.03 (m, 2H), 7.72-7.68 (m, 1H), 7.59-7.55 (m, 2H), 5.96 (s, 2H). **^{13}C NMR** (100 MHz, DMSO-d6): 193.24, 158.24, 156.80, 154.64, 134.74, 129.47, 129.11, 128.51, 103.81, 90.39, 57.78. **IR** (KBr) cm^{-1}: 3455, 3302 (NH_2), 1706 (CO). **MS** (ESI): *m/z* = 380.6 $[M+H]^+$. **Anal. calcd.** for $C_{13}H_{10}N_5OI$: C 41.18, H 2.66, N 18.47; **found**: C 41.27, H 2.91, N 18.13.

*4.2.5 2-(4-Amino-3-iodo-1H-pyrazolo[3,4-d]pyrimidin-1-yl)-1-phenylethanol **10**.*

$NaBH_4$ (1.08 g, 28.48 mmol) was added to a solution of 2-(4-amino-3-iodo-1*H*-pyrazolo[3,4-*d*]pyrimidin-1-yl)-1-phenylethanone **9** (600 mg, 1.58 mmol) in MeOH (150 mL), and the mixture was stirred at 0 °C for 3 h. Water (40 mL) was added and the mixture was stirred for other 10 minutes. Then MeOH was evaporated and the suspension was extracted with CH_2Cl_2 (3 x 50 mL), the organic solution was washed with water (100 mL), dried ($MgSO_4$), filtered, and concentrated under reduced pressure. The crude oil was purified by column chromatography (silica gel 220-440 mesh, 60 Å) using CH_2Cl_2/MeOH (95:5) as the eluant to afford the pure product **10**. **Yield**: 31%. White solid. **Mp**: 186-188 °C. **^{1}H NMR** (400 MHz, $CDCl_3$): δ (ppm) 8.08 (s, 1H), 7.24-7.09 (m, 5H), 5.01-4.98 (m, 1H), 4.52-4.46 (m, 1H), 4.28-4.23 (m, 1H). **^{13}C NMR** (100 MHz, $CDCl_3$): 157.07, 154.93, 154.05, 141.19, 128.71, 128.08, 126.19, 104.00, 86.98, 72.86, 55.85. **IR** (KBr) cm^{-1}: 3500-300 (OH), 3465, 3294 (NH_2). **MS** (ESI): *m/z* = 382.2 $[M+H]^+$. **Anal. calcd.** for $C_{13}H_{12}N_5OI$: C 40.96, H 3.17, N 18.37; **found** C 40.89, H 3.32, N 18.58.

*4.2.6 1-(2-Chloro-2-phenylethyl)-3-iodo-1H-pyrazolo[3,4-d]pyrimidin-4-amine **11**.*

$SOCl_2$ (230 µL, 3.2 mmol) was added dropwise to a solution of 2-(4-amino-3-iodo-1*H*-pyrazolo[3,4-*d*]pyrimidin-1-yl)-1-phenylethanol **10** (370 mg, 0.97 mmol) in anhydrous CH_2Cl_2 (15 mL), and the reaction was stirred at room temperature for 12 h under nitrogen atmosphere. Water (10 mL) and 1 N NaOH (2 mL) were added with caution and the aqueous phase was extracted with CH_2Cl_2 (3 x 15 mL). Then the organic phase was washed with water (30 mL), brine (30 mL), dried (Na_2SO_4) and concentrated under reduced pressure. The crude product was purified by column chromatography (silica gel 220-440 mesh, 60 Å) using CH_2Cl_2/MeOH (95:5) as the eluant to afford the pure product **11**. **Yield**: 33%. White solid. **Mp**: 204-209 °C. **^{1}H NMR** (200 MHz, $CDCl_3$): δ (ppm) 8.34 (s, 1H), 7.57-7.29 (m, 5H), 6.43 (br s, 2H), 5.57-5.50 (m, 1H), 5.06-4.94 (m, 1H), 4.79-4.69 (m, 1H). **^{13}C NMR** (50 MHz, $CDCl_3$): 156.96, 154.84, 154.03, 141.12, 128.65, 127.03, 126.09, 104.00, 85.97, 72.43, 55.37. **IR** (KBr) cm^{-1}: 3452, 3301 (NH_2). **MS** (ESI): *m/z* = 400.4 $[M+H]^+$. **Anal. calcd.** for $C_{13}H_{11}N_5ICl$: C 39.07, H 2.27, N 17.53; **found** C 38.89, H 2.89, N 17.62.

*4.2.7 General procedure for the synthesis of final compounds **2g,h**.*

(Hydroxymethyl)phenylboronic acid (76 mg, 0.5 mmol), Cs_2CO_3 (122 mg, 0.375 mmol) and [1,1′-bis(diphenylphosphino)ferrocene]dichloropalladium (II) ($Pd(dppf)Cl_2$) (5 mg, 10 mol%) were added to a solution of the suitable intermediate **10** or **11** (0.125 mmol) in 1,2-dimethoxyethane (DME) (2 mL) and H_2O (0.3 mL). Then the mixture was stirred at 90° C for 14 h. After cooling to room temperature, water (5 mL) was added and the aqueous suspension was extracted with AcOEt (3 x 5 mL). The organic layers were washed with water (15 mL), dried ($MgSO_4$), filtered, and concentrated under reduced pressure. The crude product was purified by column chromatography (silica gel 220-440 mesh, 60 Å) using AcOEt/n-hexane (95:5) as the eluant to afford the pure products **2g** and **2h**.

4.2.7.1 2-{4-Amino-3-[4-(hydroxymethyl)phenyl]-1H-pyrazolo[3,4-d]pyrimidin-1-yl}-1-phenylethanol

*(**2g**).* **Yield**: 25%. White solid. **Mp**: 204-206 °C. **^{1}H NMR** (400 MHz, $CDCl_3$): δ (ppm) 8.36 (s, 1H), 7.68-7.66 (m, 2H), 7.56-7.48 (m, 4H), 7.38-7.26 (m, 3H), 5.69 (br s, 2H), 5.30-5.28 (m, 1H), 4.80 (s, 2H), 4.74-4.60 (m, 2H). **^{13}C NMR** (100 MHz, $CDCl_3$): 156.07, 153.50, 153.21, 137.69, 135.34, 132.61, 129.11, 128.82, 127.71, 127.35, 126.42, 121.43, 117.91, 100.25, 60.29, 54.10. **IR** (KBr) cm^{-1}: 3500-300 (OH), 3501, 3320 (NH_2). **MS** (ESI): *m/z* = 362.4 $[M+H]^+$. **Anal. calcd.** for $C_{20}H_{19}N_5O_2$: C 66.47, H 5.30, N 19.38; **found** C 66.67, H 5.22, N 19.49.

4.2.7.2 *{4-[4-Amino-1-(2-chloro-2-phenylethyl)-1H-pyrazolo[3,4-d]pyrimidin-3-yl]phenyl}methanol (**2h**).* **Yield**: 57%. White solid. **Mp**: 220-223 °C. **^{1}H NMR** (200 MHz, $CDCl_3$): δ (ppm) 8.38 (s, 1H), 7.67-7.66 (m, 2H), 7.55-7.54 (m, 2H), 7.49-7.47 (m, 2H), 7.36-7.7.31 (m, 3H), 5.62-5.59 (m, 1H), 5.47 (br s, 2H), 5.08-5.03 (m, 1H), 4.82-4.80 (m, 3H). **^{13}C NMR** (50 MHz, $CDCl_3$): 156.12, 153.55, 153.23, 137.72, 135.39, 132.62, 129.09, 128.84, 127.70, 127.39, 126.44, 121.46, 117.93, 100.35, 60.32, 54.08. **IR** (KBr) cm^{-1}: 3500-300 (OH), 3500, 3319 (NH_2). **MS** (ESI): *m/z* = 380.1 $[M+H]^+$. **Anal. calcd.** for $C_{20}H_{18}N_5OCl$: C 63.24, H 4.78, N 18.44; **found** C 63.27, H 5.11, N 18.09.

*4.2.8 3-Iodo-1-(2-phenylethyl)-1H-pyrazolo[3,4-d]pyrimidin-4-amine **12b**.*

K_2CO_3 (600 mg, 4.34 mmol) was added to a solution of 3-iodo-1*H*-pyrazolo[3,4-*d*]pyrimidin-4-amine **8** (400 mg, 1.53 mmol) in dry DMF (5 mL), and the mixture was heated at 50-70 °C for 1 h. Then (2-bromoethyl)benzene (426 mg, 2.30 mmol) was added, and the reaction was stirred at 130 °C for 18 h. After cooling to room temperature, water was added (20 mL) and the precipitated solid was recrystallized from absolute ethanol to obtain **12b**. **Yield**: 42%. Light brown solid. **Mp**: 192-193 °C. **^{1}H NMR** (400 MHz, $CDCl_3$): δ (ppm) 8.28 (s, 1H), 7.25-7.20 (m, 5H), 6.11 (br s, 2H), 4.59 (t, *J* = 8.0 Hz, 2H), 3.20 (t, *J* = 8.0 Hz, 2H). **^{13}C NMR** (100 MHz, $CDCl_3$): 159.51, 153.41, 153.07, 135.91, 130.75, 128.91, 128.72, 128.56, 93.36, 49.41, 31.10. **IR** (KBr) cm^{-1}: 3481, 3358 (NH_2). **MS** (ESI): *m/z* = 365.9 $[M+H]^+$. **Anal. calcd.** for $C_{13}H_{12}N_5I$: C 42.76, H, 3.31 N 19.18; **found**: C 42.62, H 3.70, N 18.91.

*4.2.9 General procedure for the synthesis of final compounds **2i-l**.*

The suitable boronic acid (1.08 mmol) was added to a suspension of the intermediates **12a** or **12b** (0.27 mmol) in dry toluene (5 mL), and the mixture was stirred at room temperature under nitrogen atmosphere for 10 min. Then Cs_2CO_3 (350 mg, 1.07 mmol) and [1,1′-bis(diphenylphosphino)ferrocene]dichloropalladium (II) ($Pd(dppf)Cl_2$) (20 mg, 10 mol%) were added. The reaction was stirred at 90 °C for 14 h. After cooling to room temperature, water (10 mL) was added and the aqueous suspension was extracted with AcOEt (3 × 10 mL). The organic phase was washed with water (10 mL) and brine (10 mL), dried (Na_2SO_4), and concentrated under reduced pressure. The crudes were purified by column chromatography (silica gel 0.060-0.200 mm, 40 Å) using a mixture of CH_2Cl_2/MeOH (95:5) as the eluent to afford compounds **2i-l**.

4.2.9.1 *3-(4-Fluorophenyl)-1-(2-phenylpropyl)-1H-pyrazolo[3,4-d]pyrimidin-4-amine (**2i**).* **Yield**: 50%. Yellow solid. **Mp**: 210-212 °C. **^{1}H NMR** (400 MHz, $CDCl_3$): δ (ppm) 8.34 (s, 1H), 7.65-7.61 (m, 2H), 7.26-7.16 (m, 7H), 5.88 (br s, 2H), 4.57-4.54 (m, 2H), 3.63-3.57 (m, 1H), 1.28 (d, *J* = 6.8 Hz,

3H). **^{13}C NMR** (100 MHz, $CDCl_3$): 163.43, 159.52, 153.86, 153.42, 153.01, 144.21, 132.68, 130.71, 128.95, 128.64, 127.73, 127.18, 115.93, 52.32, 41.67, 19.48. **IR** (KBr) cm^{-1}: 3463, 3420 (NH_2). **MS** (ESI): *m/z* = 348.2 $[M+H]^+$. **Anal. calcd.** for $C_{20}H_{18}N_5F$: C 69.15, H 5.22, N 20.16; **found**: C 69.17, H 5.37, N 20.39.

4.2.9.2 *3-(4-Nitrophenyl)-1-(2-phenylpropyl)-1H-pyrazolo[3,4-d]pyrimidin-4-amine (**2j**).* **Yield**: 23%. Yellow solid. **Mp**: 255-257 °C. **^{1}H NMR** (400 MHz, $CDCl_3$): δ (ppm) 8.33 (s, 1H), 7.84-7.82 (m, 2H), 7.26-7.22 (m, 7H), 6.21 (br s, 2H), 4.63-4.61 (m, 2H), 3.60-3.58 (m, 1H), 1.32 (d, *J* = 6.4 Hz, 3H). **^{13}C NMR** (100 MHz, $CDCl_3$): 159.55, 153.84, 153.40, 152.93, 144.28, 132.72, 131.12, 130.74, 128.92, 128.61, 127.17, 127.18, 117.15, 52.35, 41.69, 19.52. **IR** (KBr) cm^{-1}: 3470, 3312 (NH_2), 1567, 1350 (NO_2). **MS** (ESI): *m/z* = 375.0 $[M+H]^+$. **Anal. calcd.** for $C_{20}H_{18}N_6O_2$: C 64.16, H 4.85, N 22.45; **found**: C 64.45, H 4.68, N 22.11.

4.2.9.3 *3-(4-Chlorophenyl)-1-(2-phenylethyl)-1H-pyrazolo[3,4-d]pyrimidin-4-amine (**2k**)* [40]. **Yield**: 48%. Light brown solid. **Mp**: 190-191 °C. **^{1}H NMR** (400 MHz, $CDCl_3$): δ (ppm) 8.36 (s, 1H), 7.64-7.62 (m, 2H), 7.53-7.51 (m, 2H), 7.27-7.20 (m, 5H), 5.49 (br s, 2H), 4.67 (t, *J* = 8.0 Hz, 2H), 3.27 (t, *J* = 8.0 Hz, 2H). **^{13}C NMR** (100 MHz, $CDCl_3$): 159.54, 153.82, 153.40, 152.97, 135.91, 135.72, 132.67, 130.74, 129.10, 128.92, 128.76, 128.68, 128.54, 49.43, 31.15. **IR** (KBr) cm^{-1}: 3474, 3323 (NH_2). **MS** (ESI): *m/z* = 350.0 $[M]^+$. **Anal. calcd.** for $C_{19}H_{16}N_5Cl$: C 65.24, H 4.61, N 20.02; **found**: C 65.43, H 5.00, N 19.97.

4.2.9.4 *3-(4-Methylphenyl)-1-(2-phenylethyl)-1H-pyrazolo[3,4-d]pyrimidin-4-amine (**2l**).* **Yield**: 50%. Yellow solid. **Mp**: 173-174°C. **^{1}H NMR** (400 MHz, $CDCl_3$): δ (ppm) 8.34 (s, 1H), 7.58-7.56 (m, 2H), 7.35-7.33 (m, 2H), 7.29-7.18 (m, 5H), 5.63 (br s, 2H), 4.66 (t, *J* = 8.0 Hz, 2H), 3.27 (t, *J* = 8.0 Hz, 2H), 2.46 (s, 3H). **^{13}C NMR** (100 MHz, $CDCl_3$): 159.58, 153.77, 153.43, 153.21, 139.82, 135.97, 132.64, 130.72, 129.33, 128.92, 128.76, 128.55, 125.22, 49.49, 31.17, 21.37. **IR** (KBr) cm^{-1}: 3477, 3321 (NH_2). **MS** (ESI): *m/z* = 330.0 $[M+H]^+$. **Anal. calcd.** for $C_{20}H_{19}N_5$: C 72.93, H 5.81, N 21.26; **found**: C 72.69, H 5.59, N 21.25.

4.3 In vitro inhibition assay

Tyrosine kinases were purchased from Merck-Millipore. Reaction were performed according to manufacturer's instructions with minor modifications. All substrates were used at least at twice the concentration of apparent Km. In details, Src and Fyn reactions were performed using 250 μM Src-peptide (KVEKIGEGTYGVVYK). 100 μM ATP and 0.00087% NP-40. Lyn reaction was performed using 200 μM Src-peptide, 40 μM ATP and 0.0013% NP-40. Blk reaction was performed using 200 μM Src-Peptide, 100 μM ATP and 0.0013 % NP-40. All reactions were performed using 0.1 μL of γ–P33 ATP, 10-50 ng of enzyme, 10% DMSO in 10 μL at 30 °C for 10 min. To avoid peptide adsorption to the plastic surface, protein low-binding tubes were used. Reactions were stopped by adding 5 μl of phosphoric acid 0.8%. Aliquots (10 μL) were then transfer into a P30 Filtermat (PerkinElmer), washed five times with 75 mM phosphoric acid and once with acetone for 5 min.

The filter was dried and transferred to a sealable plastic bag and 4 mL scintillation cocktail was added. Spotted reactions were read in a scintillation counter (Trilux. Perkinelmer). Data were plotted using GraphPad Prism 5.0. ID_{50} values were obtained according to Equation (1).

$v = V/\{1+(I/ID_{50})\}$ (1)

where v is the measured reaction velocity. V is the apparent maximal velocity in the absence of inhibitor. I is the inhibitor concentration, and ID_{50} is the 50% inhibitory dose. Si308 was assumed to act as a fully ATP-competitive inhibitor. Therefore, K_i values were calculated accordingly to equation (2).

$K_i = ID_{50}/(1+ K_m/[S])$ (2)

where K_i is the affinity of the inhibitor to the enzyme, S is the ATP concentration and K_m is the affinity of ATP calculated accordingly to Michaelis-Menten equation. Experimentally calculated K_m values are 102 μM, 39.9 μM, and 120.9 μM respectively for Fyn, Lyn, and Blk.

4.4 Cell lines and compounds

Established human cell lines derived from GCB-DLBCL (DOHH2, FARAGE, SU-DHL-6 and SU-DHL-8), from CTCL (HUT-78, H9 and HH) and PTCL (FE-PD) were cultured in culture RPMI-1640 media supplemented with fetal bovine serum (10%). Penicillin-Streptomycin-Neomycin (~5.000 units penicillin, 5 mg streptomycin and 10 mg neomycin/mL, Sigma) and L-glutamine (1%). Cell lines were authenticated for cell identity and for Interspecies contamination (IDEXX BioResearch, Ludwigsburg, Germany). All compounds were provided by Lead Discovery Siena (LDS) and dissolved in dimethyl sulphoxide (DMSO) to obtain a stock concentration of 10 mM.

4.5 Cell proliferation and cell cycle analysis

The anti-proliferative activity of 14 compounds was assessed by using MTT, as previously described [41]. Cell cycle distribution was evaluated on cells treated with DMSO or different doses of compound **2h**: the percentages of cells in G1, S and G2/M phases of the cell cycle were determined using the Watson Pragmatic model and the FlowJo software (TreeStar Inc., Ashland, OR, USA).

4.6 ADME in vitro

4.6.1 Chemicals.

All solvents, reagents, NADPH, D-glucose-6-phosphate, glucose-6-phosphate dehydrogenase, L-α-phosphatidylcholine, were from Sigma-Aldrich Srl (Milan, Italy). Dodecane was purchased from Fluka (Milan, Italy). HLM pooled male donors (20 mg/mL) were purchased from BD Gentest-Biosciences (San Jose, California). Milli-Q quality water (Millipore, Milford, MA, USA) was used. Hydrophobic filter plates (MultiScreen-IP, Clear Plates, 0.45 μm diameter pore size), 96-well micro-plates, and 96-well UV-transparent microplates were obtained from Millipore (Bedford, MA, USA).

4.6.2 UV/LC-MS methods.

LC analyses for water solubility were performer by LC-MS-MS system consisted of a Varian apparatus (Varian Inc) including a vacuum solvent degassing unit, two pumps (212-LC), a Triple

Quadrupole MSD (Mod. 320-LC) mass spectrometer with ES interface and Varian MS Workstation System Control Vers. 6.9 software. Chromatographic separation was obtained using a Pursuit C18 column (50 x 2.0 mm) (Varian) with 3 µm particle size and gradient elution with a binary solution; (eluent A: ACN, eluent B: Water, both eluents were acidified with formic acid 0.1%). The analysis started with 5% of A (from t = 0 to t = 3 min), then A was increased to 95% (from t = 3 to t = 12 min), then kept at 95% (from t = 12 to t = 20 min) and finally return to 5% of eluent A in 1.0 min. The flow rate was 0.2 mL min^{-1} and injection volume was 5 µL. The instrument operated in positive mode and parameters were: detector 1850 V, drying gas pressure 25.0 psi, desolvation temperature 300.0 °C, nebulizing gas 45.0 psi, needle 5000 V and shield 600 V. Nitrogen was used as nebulizer gas and drying gas. Collision induced dissociation was performed using Argon as the collision gas at a pressure of 1.8 mTorr in the collision cell. The transitions as well as the capillary voltage and the collision energy used are appropriated for each tested compound. Quantification of the single compound was made by comparison with apposite calibration curves realized with standard solutions in methanol.

LC analyses of PAMPA and metabolic stability were performed by Agilent 1100 UV/LC-MS system (G1946C) (Agilent Technologies, Palo Alto, CA) constituted by a vacuum solvent degassing unit, a binary high-pressure gradient pump, a 1100 series UV detector and a 1100 MSD model VL benchtop mass spectrometer. The Agilent 1100 series mass spectra detection (MSD) single-quadrupole instrument was equipped with the orthogonal spray API-ES (Agilent Technologies, Palo Alto, CA). Nitrogen was used as nebulizing and drying gas. The pressure of the nebulizing gas, the flow of the drying gas, the capillary voltage, the fragmentor voltage and the vaporization temperature were set at 40 psi, 9 L/min, 3000 V, 70 V and 350 °C, respectively. UV detection was monitored at 254 nm. The HPLC-ESI-MS determination was performed by operating the MSD in the positive ion mode. Spectra were acquired over the scan range m/z 105-1500 using a step size of 0.1 u. Chromatographic analysis were performed using a Phenomenex Kinetex C18-100A column (150 x 4.6 mm, 5 µm particle size) at room temperature. Analysis were carried out using gradient elution of a binary solution; (eluent A: ACN, eluent B: Water, both eluents were acidified with formic acid 0.1%). The analysis started with 5% of A (from t = 0 to t = 3 min), then A was increased to 95% (from t = 3 to t = 12 min), then kept at 95% (from t = 12 to t = 20 min) and finally return to 5% of eluent A in 1.0 min. The analyses were performed at a flow rate of 0.6 mL/min with 20 µL as injection volume.

4.6.3 Water Solubility.

Each solid compound (1 mg) was added to 1 mL of water. Each sample was mixed at 20 °C, in a shaker water bath for 24 h. The resulting suspension was filtered through a 0.45 µm nylon filter (Acrodisc). The concentration of compound in solution was determined by UV/LC-MS-MS (performed in triplicate) by comparison with the appropriate calibration curve that was obtained from samples of the compound dissolved in methanol at different concentrations.

4.6.4 Parallel Artificial Membrane Permeability Assay (PAMPA).

Each 'donor solution' was prepared from a solution of the appropriate compound (DMSO, 1 mM) diluted with phosphate buffer (pH 7.4, 25.0 mM) up to a final concentration of 500 μM. The donor wells were filled with 150 μL of 'donor solution'. The filters were coated with 5 μL of a solution of phosphatidylcholine in dodecane 1% (w/v) and filled with 300 μL of 'acceptor solution' (50% v/v DMSO and phosphate buffer). The sandwich plate was assembled and incubated for 5 hours at r.t. under gentle shaking. After the incubation time, the sandwich was disassembled and the amount of compound in both the donor and acceptor wells was measured by UV/LC-MS. Permeability (P_{app}) was calculated according to the following equation (3) [42]:

$P_{app} = - (V_D V_A)/ (V_D V_A) At \cdot \ln(1-r)$ (3)

where V_A is the volume in the acceptor well (cm^3), V_D is the volume in the donor well (cm^3), A is the "effective area" of the membrane (cm^2), t is the incubation time (s) and r the ratio between drug concentration in the acceptor and equilibrium concentration of the drug in the total volume (V_D+V_A). Drug concentration was estimated by using the peak area integration.

Membrane Retention (MR) was calculated according to the following equation (4):

$\%MR = \{r-(D+A)/C\} \cdot 100$

Where r is the ratio between drug concentration in the acceptor and equilibrium concentration of the drug in the total volume (V_D+V_A), D, A and C represent the drug concentration in donor and, acceptor compartment respectively, C is the equilibrium concentration. The experiments were conducted in triplicate.

4.6.5 Metabolic Stability in HLM (Human Liver Microsomes).

The incubation mixture (total volume of 500 μL) was constituted by the following components: human liver microsomes (0.2 mg/mL, 5 μL), a NADPH regenerating system (NADPH 0.2 mM, $NADPH^+$ 1 mM, D-glucose-6-phosphate 4 mM, 4 unit/mL glucose-6-phosphate dehydrogenase and $MgCl_2$ 48 mM), 50 μM of each compound in DMSO and phosphate buffer (pH 7.4, 25 mM, up to a final volume of 500 μL). The mixture was incubated at 37 °C for 1 h. The reaction was cooled down and quenched with acetonitrile (1.0 mL). After centrifugation (104 rpm, 10 min), the surnatant was taken, dried under nitrogen flow, suspended in 100 μL of methanol and analyzed by UV/LC-MS to determine the percentage of compound that was not metabolized. The experiments were conducted in triplicate.

Conflicts of Interest

'Declarations of interest: none'

Role of the founding source

This work was supported by AIRC (Associazione Italiana per la Ricerca sul Cancro) Grant IG-2015, code 17677. GM was supported by AIRC Investigator Grants IG15868 and IG20762. EC and MK were supported by AIRC Grant MFAG2016 1881.

Acknowledgments

We thank AIRC (Associazione Italiana per la Ricerca sul Cancro) for the financial support, Grant IG-2015, code 17677, Investigator Grants IG15868 and IG20762 and Grant MFAG2016 1881. We also thank COST Action CA15135 for networking contribution.

REFERENCES

[1] R.C. Lynch, D. Gratzinger, R.H. Advani, Clinical Impact of the 2016 Update to the WHO Lymphoma Classification, Curr. Treat. Options Oncol. 18 (2017), 45. doi:10.1007/s11864-017-0483-z.

[2] S.H. Swerdlow, E. Campo, S.A. Pileri, N.L. Harris, H. Stein, R. Siebert, R. Advani, M. Ghielmini, G.A. Salles, A.D. Zelenetz, E.S. Jaffe, The 2016 revision of the World Health Organization classi fication of lymphoid neoplasms, 127 (2008) 2375–2391. doi:10.1182/blood-2016-01-643569.

[3] M.J. Matasar, A.D. Zelenetz, Overview of Lymphoma Diagnosis and Management, Radiol. Clin. North Am. 46 (2008) 175–198. doi:10.1016/j.rcl.2008.03.005.

[4] https://www.cancer.org/cancer/lymphoma.html (accessed April 17, 2019).

[5] K. Ekström-Smedby, Epidemiology and etiology of non-Hodgkin lymphoma - A review, Acta Oncol. 45 (2006) 258–271. doi:10.1080/02841860500531682.

[6] B.C.H. Chiu, D.D. Weisenburger, An update of the epidemiology of non-Hodgkin's lymphoma, Clin. Lymphoma. 4 (2003) 161–168. doi:10.3816/CLM.2003.n.025.

[7] L. Pasqualucci, R. Dalla-Favera, Genetics of diffuse large B-cell lymphoma, Blood. 131 (2018) 2307 LP-2319. doi:10.1182/blood-2017-11-764332.

[8] J.S. Van Arnam, M.S. Lim, K.S.J. Elenitoba-Johnson, Novel insights into the pathogenesis of T-cell lymphomas, Blood. 131 (2018) 2320 LP-2330. doi:10.1182/blood-2017-11-764357.

[9] J.D. Phelan, R.M. Young, D.E. Webster, S. Roulland, G.W. Wright, M. Kasbekar, A.L. Shaffer 3rd, M. Ceribelli, J.Q. Wang, R. Schmitz, M. Nakagawa, E. Bachy, D.W. Huang, Y. Ji, L. Chen, Y. Yang, H. Zhao, X. Yu, W. Xu, M.M. Palisoc, R.R. Valadez, T. Davies-Hill, W.H. Wilson, W.C. Chan, E.S. Jaffe, R.D. Gascoyne, E. Campo, A. Rosenwald, G. Ott, J. Delabie, L.M. Rimsza, F.J. Rodriguez, F. Estephan, M. Holdhoff, M.J. Kruhlak, S.M. Hewitt, C.J. Thomas, S. Pittaluga, T. Oellerich, L.M. Staudt, A multiprotein supercomplex controlling oncogenic signalling in lymphoma, Nature. 560 (2018) 387–391. doi:10.1038/s41586-018-0290-0.

[10] E. Battistello, N. Katanayeva, E. Dheilly, D. Tavernari, M.C. Donaldson, L. Bonsignore, M. Thome, A.L. Christie, M.A. Murakami, O. Michielin, G. Ciriello, V. Zoete, E. Oricchio, Pan-SRC kinase inhibition blocks B-cell receptor oncogenic signaling in non-Hodgkin lymphoma, Blood. 131 (2018) 2345–2356. doi:10.1182/blood-2017-10-809210.

[11] C. Scuoppo, W. Jiguang, M. Persaud, S. Mittan, L. Pasqualucci, R. Rabadan, C. Grandori, R. Dalla-Favera, Repurposing Dasatinib for Ibrutinib-Resistant Diffuse Large B-Cell lymphoma, Blood. 130 (2017) 3843.

[12] M.L. Cann, L.E. Herring, L.L. Haar, T.S.K. Gilbert, D. Goldfarb, K.L. Richards, L.M. Graves, D.S. Lawrence, Dasatinib Is Preferentially Active in the Activated B-Cell Subtype of Diffuse Large B-cell lymphoma, J. Proteome Res. 18 (2019) 522–534.

doi:10.1021/acs.jproteome.8b00841.

[13] T. Palomero, L. Couronné, H. Khiabanian, M.-Y. Kim, A. Ambesi-Impiombato, A. Perez-Garcia, Z. Carpenter, F. Abate, M. Allegretta, J.E. Haydu, X. Jiang, I.S. Lossos, C. Nicolas, M. Balbin, C. Bastard, G. Bhagat, M.A. Piris, E. Campo, O.A. Bernard, R. Rabadan, A.A. Ferrando, Recurrent mutations in epigenetic regulators, RHOA and FYN kinase in peripheral T cell lymphomas, Nat. Genet. 46 (2014) 166. https://doi.org/10.1038/ng.2873.

[14] T. Krejsgaard, C.S. Vetter-Kauczok, A. Woetmann, H. Kneitz, K.W. Eriksen, P. Lovato, Q. Zhang, M.A. Wasik, C. Geisler, E. Ralfkiaer, J.C. Becker, N. Ødum, Ectopic expression of B-lymphoid kinase in cutaneous T-cell lymphoma, Blood. 113 (2009) 5896–5904. doi:10.1182/blood-2008-09-181024.

[15] S. Fredholm, D.L. Petersen, T. Hu, C.M. Bonefeld, A. Willerslev-Olsen, J. V Olsen, C. Francavilla, M. Zhang, N.A. Sibbesen, M.H. Andersen, T. Krejsgaard, J. Berthelsen, A. Woetmann, C. Geisler, N. Odum, M.A. Wasik, B-lymphoid tyrosine kinase (Blk) is an oncogene and a potential target for therapy with dasatinib in cutaneous T-cell lymphoma (CTCL), Leukemia. 28 (2014) 2109–2112. doi:10.1038/leu.2014.192.

[16] I. Laurenzana, A. Caivano, F. La Rocca, S. Trino, L. De Luca, F. D'Alessio, S. Schenone, G. Falco, M. Botta, L. Del Vecchio, P. Musto, A pyrazolo[3,4-d]pyrimidine compound reduces cell viability and induces apoptosis in different hematological malignancies, Front. Pharmacol. 7 (2016) 1–9. doi:10.3389/fphar.2016.00416.

[17] C. Tintori, G. La Sala, G. Vignaroli, L. Botta, A.L. Fallacara, F. Falchi, M. Radi, C. Zamperini, E. Dreassi, L. Dello Iacono, D. Orioli, G. Biamonti, M. Garbelli, A. Lossani, F. Gasparrini, T. Tuccinardi, I. Laurenzana, A. Angelucci, G. Maga, S. Schenone, C. Brullo, F. Musumeci, A. Desogus, E. Crespan, M. Botta, Studies on the ATP Binding Site of Fyn Kinase for the Identification of New Inhibitors and Their Evaluation as Potential Agents against Tauopathies and Tumors, J. Med. Chem. 58 (2015) 4590–4609. doi:10.1021/acs.jmedchem.5b00140.

[18] C. Tintori, A.L. Fallacara, M. Radi, C. Zamperini, E. Dreassi, E. Crespan, G. Maga, S. Schenone, F. Musumeci, C. Brullo, A. Richters, F. Gasparrini, A. Angelucci, C. Festuccia, S. Delle Monache, D. Rauh, M. Botta, Combining X-ray Crystallography and Molecular Modeling toward the Optimization of Pyrazolo[3,4-d]pyrimidines as Potent c-Src Inhibitors Active in Vivo against Neuroblastoma, J. Med. Chem. 58 (2015) 347–361. doi:10.1021/jm5013159.

[19] C. Tintori, I. Laurenzana, F. LaRocca, F. Falchi, F. Carraro, A. Ruiz, J.A. Esté, M. Kissova, E. Crespan, G. Maga, M. Biava, C. Brullo, S. Schenone, M. Botta, Identification of Hck Inhibitors As Hits for the Development of Antileukemia and Anti-HIV agents, ChemMedChem. 8 (2013) 1353–1360. doi:10.1002/cmdc.201300204.

[20] T.A. Halgren, R.B. Murphy, R.A. Friesner, H.S. Beard, L.L. Frye, W.T. Pollard, J.L. Banks, Glide: A New Approach for Rapid, Accurate Docking and Scoring. 2. Enrichment Factors in

Database Screening, J. Med. Chem. 47 (2004) 1750–1759. doi:10.1021/jm030644s.

[21] T. Kinoshita, M. Matsubara, H. Ishiguro, K. Okita, T. Tada, Structure of human Fyn kinase domain complexed with staurosporine, Biochem. Biophys. Res. Commun. 346 (2006) 840–844. doi:10.1016/j.bbrc.2006.05.212.

[22] H.T. Kim, Crystal structure of Lyn kinase domain in complex with N-(1H-indazol-6-yl)-8-(piperidin-4-yloxy)-6-propylquinazolin-2-amine, https://www.rcsb.org/structure/5XY1 (accessed April 2, 2019).

[23] M.P. Jacobson, D.L. Pincus, C.S. Rapp, T.J.F. Day, B. Honig, D.E. Shaw, R.A. Friesner, A Hierarchical Approach to All-Atom Protein Loop Prediction, Proteins Struct. Funct. Genet. 55 (2004) 351–367. doi:10.1002/prot.10613.

[24] M.P. Jacobson, R.A. Friesner, Z. Xiang, B. Honig, On the role of the crystal environment in determining protein side-chain conformations, J. Mol. Biol. 320 (2002) 597–608. doi:10.1016/S0022-2836(02)00470-9.

[25] M. Wiederstein, M.J. Sippl, ProSA-web: Interactive web service for the recognition of errors in three-dimensional structures of proteins, Nucleic Acids Res. 35 (2007) 407–410. doi:10.1093/nar/gkm290.

[26] M.J. Sippl, Recognition of errors in three-dimensional structures of proteins, Proteins Struct. Funct. Bioinforma. 17 (1993) 355–362. doi:10.1002/prot.340170404.

[27] U. Hanefeld, C.W. Rees, A.J.P. White, D.J. Williams, One-pot synthesis of tetrasubstituted pyrazoles—proof of regiochemistry, J. Chem. Soc. Perkin Trans. 1. (1996) 1545–1552. doi:10.1039/P19960001545.

[28] G. Benoit, Hydroxyalkyl hydrazines, in: Vol.6, Bull. Soc. Chim. Fr., 1939: p. p.708-715.

[29] G. Gilliland, H.M. Berman, H. Weissig, I.N. Shindyalov, J. Westbrook, P.E. Bourne, T.N. Bhat, Z. Feng, The Protein Data Bank, Nucleic Acids Res. 28 (2000) 235–242. doi:10.1093/nar/28.1.235.

[30] M. Adzhigirey, T. Day, W. Sherman, G. Madhavi Sastry, R. Annabhimoju, Protein and ligand preparation: parameters, protocols, and influence on virtual screening enrichments, J. Comput. Aided. Mol. Des. 27 (2013) 221–234. doi:10.1007/s10822-013-9644-8.

[31] A. Bateman, M.J. Martin, C. O'Donovan, M. Magrane, E. Alpi, R. Antunes, B. Bely, M. Bingley, C. Bonilla, R. Britto, B. Bursteinas, H. Bye-AJee, A. Cowley, A. Da Silva, M. De Giorgi, T. Dogan, F. Fazzini, L.G. Castro, L. Figueira, P. Garmiri, G. Georghiou, D. Gonzalez, E. Hatton-Ellis, W. Li, W. Liu, R. Lopez, J. Luo, Y. Lussi, A. MacDougall, A. Nightingale, B. Palka, K. Pichler, D. Poggioli, S. Pundir, L. Pureza, G. Qi, S. Rosanoff, R. Saidi, T. Sawford, A. Shypitsyna, E. Speretta, E. Turner, N. Tyagi, V. Volynkin, T. Wardell, K. Warner, X. Watkins, R. Zaru, H. Zellner, I. Xenarios, L. Bougueleret, A. Bridge, S. Poux, N. Redaschi, L. Aimo, G. ArgoudPuy, A. Auchincloss, K. Axelsen, P. Bansal, D. Baratin, M.C. Blatter, B. Boeckmann, J. Bolleman, E. Boutet, L. Breuza, C. Casal-Casas, E. De Castro, E. Coudert,

B. Cuche, M. Doche, D. Dornevil, S. Duvaud, A. Estreicher, L. Famiglietti, M. Feuermann, E. Gasteiger, S. Gehant, V. Gerritsen, A. Gos, N. Gruaz-Gumowski, U. Hinz, C. Hulo, F. Jungo, G. Keller, V. Lara, P. Lemercier, D. Lieberherr, T. Lombardot, X. Martin, P. Masson, A. Morgat, T. Neto, N. Nouspikel, S. Paesano, I. Pedruzzi, S. Pilbout, M. Pozzato, M. Pruess, C. Rivoire, B. Roechert, M. Schneider, C. Sigrist, K. Sonesson, S. Staehli, A. Stutz, S. Sundaram, M. Tognolli, L. Verbregue, A.L. Veuthey, C.H. Wu, C.N. Arighi, L. Arminski, C. Chen, Y. Chen, J.S. Garavelli, H. Huang, K. Laiho, P. McGarvey, D.A. Natale, K. Ross, C.R. Vinayaka, Q. Wang, Y. Wang, L.S. Yeh, J. Zhang, UniProt: The universal protein knowledgebase, Nucleic Acids Res. 45 (2017) D158–D169. doi:10.1093/nar/gkw1099.

[32] M. Sabat, J.C. VanRens, M.J. Laufersweiler, T.A. Brugel, J. Maier, A. Golebiowski, B. De, V. Easwaran, L.C. Hsieh, R.L. Walter, M.J. Mekel, A. Evdokimov, M.J. Janusz, The development of 2-benzimidazole substituted pyrimidine based inhibitors of lymphocyte specific kinase (Lck), Bioorganic Med. Chem. Lett. 16 (2006) 5973–5977. doi:10.1016/j.bmcl.2006.08.132.

[33] Schrödinger Release 2017-2: Maestro, Schrödinger, LLC, New York, NY, 2017.

[34] Schrödinger Release 2017-2: MacroModel, Schrödinger, LLC, New York, NY, 2017.

[35] J. Wang, W. Wang, P.A. Kollman, D.A. Case, Automatic atom type and bond type perception in molecular mechanical calculations, J. Mol. Graph. Model. 25 (2006) 247–260. doi:10.1016/j.jmgm.2005.12.005.

[36] D.A. Case, J. Wang, R.M. Wolf, J.W. Caldwell, P.A. Kollman, Development and testing of a general amber force field., J. Comput. Chem. 25 (2004) 1157–74. doi:10.1002/jcc.20035.

[37] J.A. Maier, C. Martinez, K. Kasavajhala, L. Wickstrom, K.E. Hauser, C. Simmerling, ff14SB: Improving the Accuracy of Protein Side Chain and Backbone Parameters from ff99SB, J. Chem. Theory Comput. 11 (2015) 3696–3713. doi:10.1021/acs.jctc.5b00255.

[38] B.R. Miller, T.D. McGee, J.M. Swails, N. Homeyer, H. Gohlke, A.E. Roitberg, MMPBSA.py: An efficient program for end-state free energy calculations, J. Chem. Theory Comput. 8 (2012) 3314–3321. doi:10.1021/ct300418h.

[39] T. Hou, J. Wang, Y. Li, W. Wang, Assessing the performance of the MM/PBSA and MM/GBSA methods. 1. The accuracy of Binding Free Energy Calculations Based on Molecular Dynamics Simulations. J. Chem. Inf. Model. 51 (2011) 69–82. doi:10.1021/ci100275a.

[40] I. Foldrx Phamaceuticals, Modulation of protein trafficking., WO2009062118, 2009.

[41] A.A. Mensah, I. Kwee, E. Gaudio, A. Rinaldi, M. Ponzoni, L. Cascione, G. Fossati, A. Stathis, E. Zucca, G. Caprini, F. Bertoni, Novel HDAC inhibitors exhibit pre-clinical efficacy in lymphoma models and point to the importance of *CDKN1A* expression levels in mediating their anti-tumor response, Oncotarget. 6 (2015). doi:10.18632/oncotarget.3239.

[42] F. Wohnsland, B. Faller, High-throughput permeability pH profile and high-throughput

alkane/water log P with artificial membranes, J. Med. Chem. 44 (2001) 923–930. doi:10.1021/jm001020e.

Supplementary Material - For Publication Online

Click here to download Supplementary Material - For Publication Online: Supplementary materials_11.docx